



**Article title:** The closure of the Vardar ocean (the western domain of the northern Neotethys) from early Middle Jurassic to Paleocene time, based on surface geology of eastern Pelagonia and the Vardar zone, biostratigraphy, and seismic-tomographic images of the mantle below the Central Hellenides

**Authors:** Rudolph Scherreiks[1], Marcelle Boudagher-Fadel[2]

**Affiliations:** Geologische Staatssammlung of the Bayerische Staatssammlung für Palaeontologie und Geologie, Germany[1], Professorial Research Fellow, Office of the Vice-Provost (Research), University College London, UK[2]

**Orcid ids:** 0000-0002-2777-1476[1], 0000-0002-2339-2444[2]

**Contact e-mail:** m.fadel@ucl.ac.uk

**License information:** This is an open access article distributed under the terms of the Creative Commons Attribution License (CC BY) 4.0 <https://creativecommons.org/licenses/by/4.0/>, which permits unrestricted use, distribution and reproduction in any medium, provided the original author and source are credited.

**Preprint statement:** This article is a preprint and has not been peer-reviewed, under consideration and submitted to UCL Open: Environment Preprint for open peer review.

**Funder:** N/A

**DOI:** 10.14324/111.444/000078.v1

**Preprint first posted online:** 27 April 2021

**Keywords:** Adria, Pelagonia, Vardar, subduction and obduction, ocean lithosphere, tectono-stratigraphy, biostratigraphy, tomographic images, ophiolite, carbonate platforms, The Environment, Climate, Built environment

1 **The closure of the Vardar ocean (the western domain of the**  
2 **northern Neotethys) from early Middle Jurassic to Paleocene time,**  
3 **based on surface geology of eastern Pelagonia and the Vardar**  
4 **zone, biostratigraphy, and seismic-tomographic images of the**  
5 **mantle below the Central Hellenides**

6  
7 Rudolph Scherreiks<sup>1</sup> Marcelle BouDagher-Fadel<sup>2</sup>

8  
9 <sup>1</sup>Geologische Staatssammlung of the Bayerische Staatssammlung für  
10 Palaeontologie und Geologie, Luisenstr. 37, 80333 Munich, Germany

11 <sup>2</sup>University College London, Office of the Vice-Provost (Research), 2  
12 Taviton Street, WC 1 H OBT, London, UK

13  
14 **Abstract**

15 Seismic tomographic images of the mantle below the Hellenides indicate  
16 that the Vardar ocean probably had a composite width of over 3000  
17 kilometres. From surface geology we know that this ocean was initially  
18 located between two passive margins: Pelagonian Adria in the west and  
19 Serbo-Macedonian-Eurasia in the east. Pelagonia was covered by a  
20 carbonate platform that accumulated, during Late Triassic to Early  
21 Cretaceous time, where highly diversified carbonate sedimentary  
22 environments evolved and reacted to the adjacent, converging Vardar  
23 ocean plate. We conceive that on the east side of the Vardar ocean, a  
24 Cretaceous carbonate platform evolved from Aptian to Maastrichtian  
25 time in the forearc basin of the Vardar supra-subduction volcanic arc  
26 complex.

27 The closure of the Vardar ocean occurred in one episode of ophiolite  
28 obduction and in two episodes of intra-oceanic subduction.

29 1. During Middle Jurassic time a 1200-kilometre slab of west Vardar  
30 lithosphere subducted beneath the supra-subduction, "Eohellenic", arc,  
31 while a 200-kilometre-wide slab obducted onto Pelagonia between  
32 Callovian and Valanginian time.

33 2. During Late Jurassic through Cretaceous time a 1700-kilometre-wide  
34 slab subducted beneath the evolving east Vardar-zone arc-complex.  
35 Pelagonia, the trailing edge of the subducting east-Vardar ocean slab,  
36 crashed and underthrust the Vardar arc complex during Paleocene time  
37 and ultimately crashed with Serbo-Macedonia. Since late Early Jurassic  
38 time, the Hellenides have moved about 3000 kilometres toward the  
39 northeast while the Atlantic Ocean spread.

41 **Key Words** Adria, Pelagonia, Vardar, subduction, obduction, tectono-  
42 stratigraphy, biostratigraphy, tomographic images, ophiolite, carbonate  
43 platforms, ocean lithosphere

## 44 **Introduction**

45 Relicts of oceanic lithosphere can be traced from the Dinarides through  
46 the Hellenides and Taurides. They bear witness to the once extensive  
47 northern Neotethys ocean (Fig 1) (Stampfli and Borel 2004; Schmid et  
48 al. 2008; Schmid et al. 2020). In this contribution, we shed new light on  
49 the palaeogeography and subduction of the Vardar branch of the  
50 Neotethys from Early Jurassic through early Palaeocene time, which we  
51 have gained from our research on the tectono-stratigraphy of the Vardar  
52 zone of Greek Macedonia and of the eastern Pelagonian zone of  
53 Northern Evvoia and the Northern Sporades (Fig.1). This surface  
54 geology is aligned with seismic tomographic images that depict two  
55 perturbations in the mantle below the central Hellenides, that we  
56 interpret as two slabs of Vardar ocean lithosphere, which sank into the  
57 mantle during two episodes of subduction. We also show that two  
58 carbonate platforms evolved, one on each side of the Vardar ocean and  
59 they reacted to and were tectonically involved with the obduction,  
60 subduction and ultimate closure of the Vardar ocean.

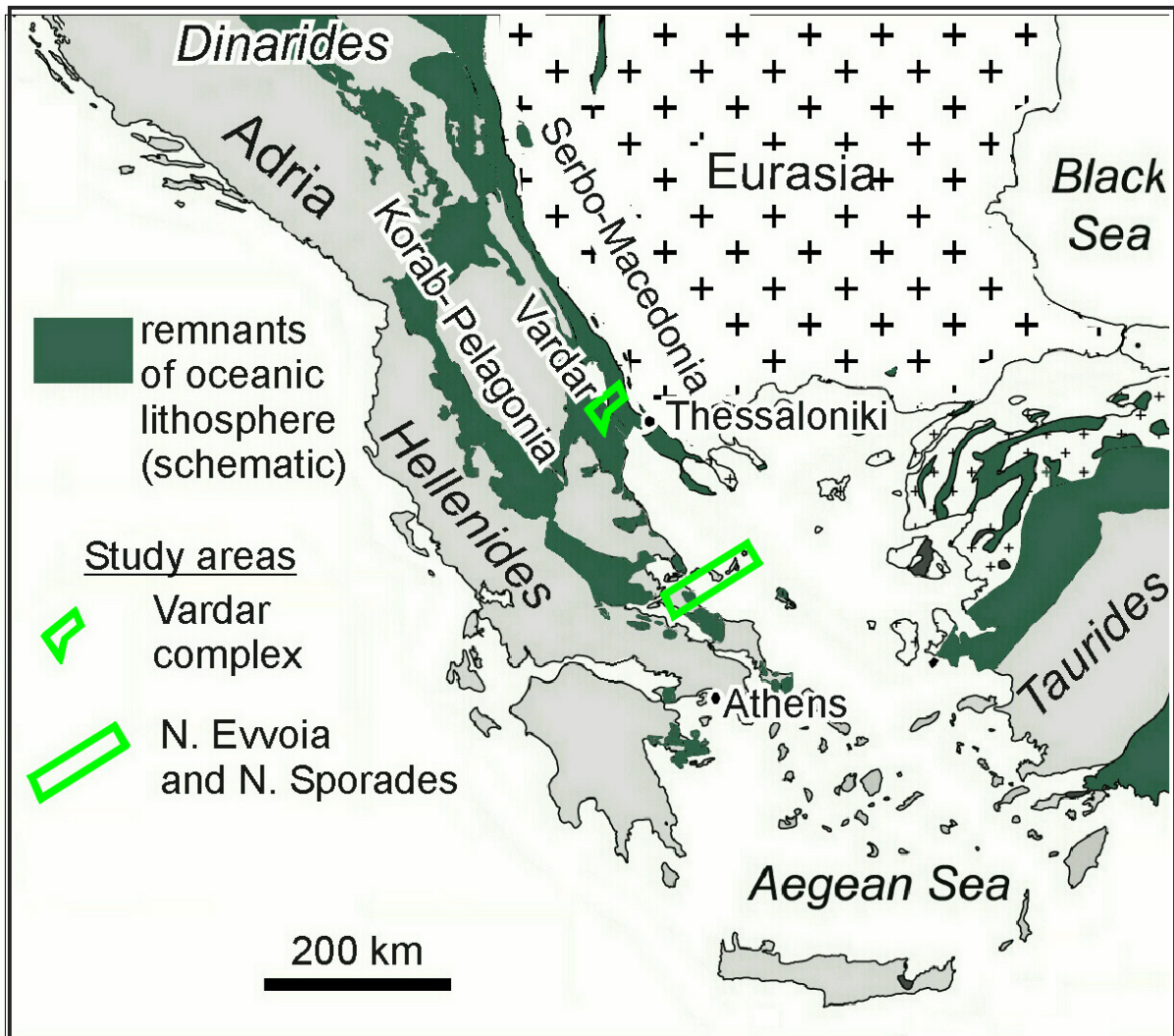
61 A time-lapse reconstruction is presented of the convergence and  
62 subduction of the Vardar ocean from Early Jurassic through early  
63 Paleocene time. We give answers to questions concerning the original  
64 width of the Vardar ocean and how closure took place and ended with  
65 Pelagonia's collision with the Vardar Island-arc-complex and the  
66 detachment and subsidence of the Vardar ocean slabs into the mantle.

## 67 **Palaeogeological Background**

### 68 ***The Neotethys, Vardar zone and some nomenclature***

69 In palaeogeographic reconstructions of the evolution of the Palaeotethys  
70 and Neotethys, Stampfli and Borel (2004) show that the northern  
71 Neotethys ocean opened as the Palaeotethys closed (fig. 2a): the Maliac  
72 ocean is a remnant of the Paleotethys, which, through intra-oceanic  
73 subduction, becomes overthrust by the Vardar ocean at the western end  
74 of the northern Neotethys. Alternatively, the Vardar ocean can simply be  
75 envisioned to have opened as a western continuation of the Neotethys  
76 (Sengor and Natal'in (1996) in Hafkingscheid (2004)).

77 In an enlightening palaeogeographic reconstruction of the Mid-Late  
78 Jurassic Vardar ocean, shown in Schmid et al. (2020) the Vardar ocean



79  
80 Fig. 1 (see figure captions)

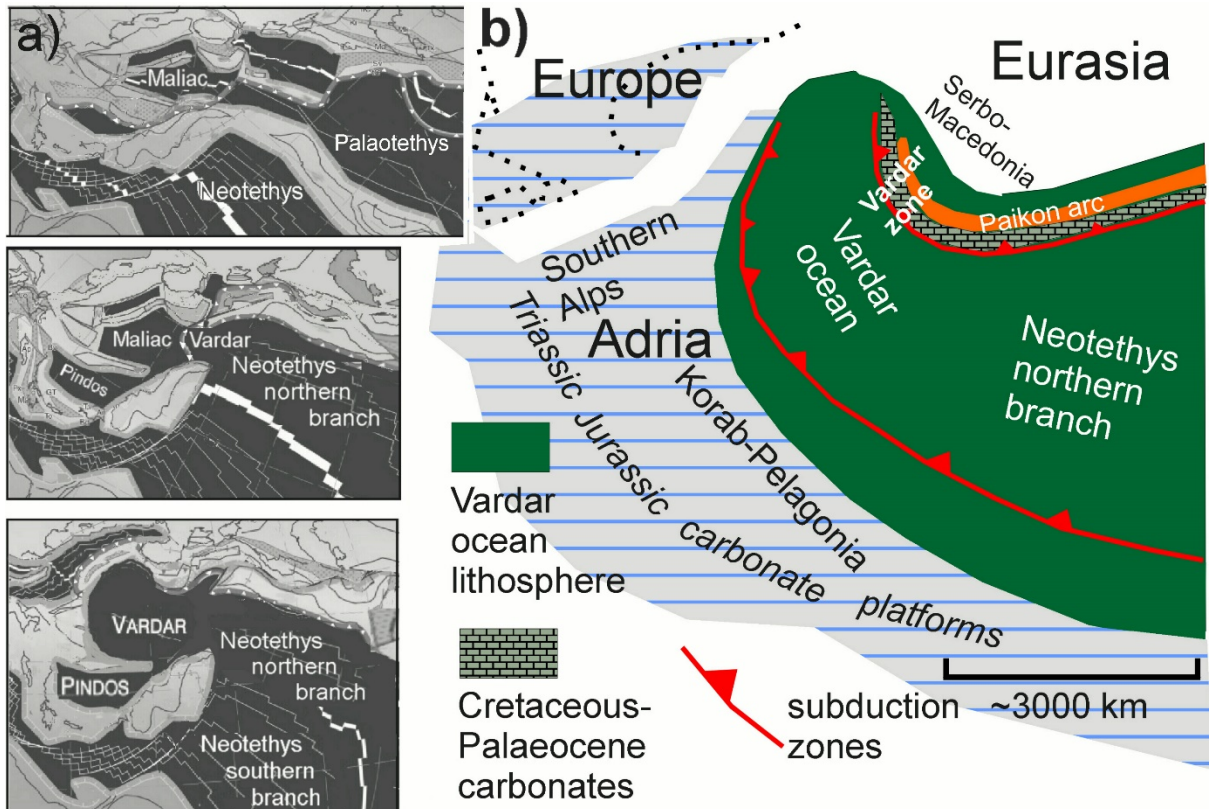
81  
82 has two eastward dipping, Intra-oceanic subduction zones and an arc  
83 complex (Fig.2b). This model infers that the Vardar ocean existed from  
84 Early Mesozoic to Late Cretaceous time (in agreement with Sharp and  
85 Robertson 2006). Our research corroborates these plate-tectonic  
86 palaeogeographic interpretations which we have proceeded to  
87 investigate both spatially and temporally. Following Schmid et al. (2008)  
88 the present contribution supports the one-ocean concept, that the Vardar  
89 ophiolites were obducted westward over the Pelagonian-Korah zone of  
90 east Adria (Fig. 2b). For other models in which western Pelagonia had  
91 plate-tectonic involvement with an inferred Pindos ocean see Sharp and  
92 Robertson (2006). Our investigations, however, have been limited to  
93 eastern Pelagonia and the Vardar zone (Fig. 1).

94  
95

96

97 **Nomenclature**

98 For nomenclatural orientation, “Vardar ocean” is the name of the  
99 western ocean domain of the northern Neotethys (Fig.2b). We agree  
100



101

102 Fig. 2 (see figure captions)

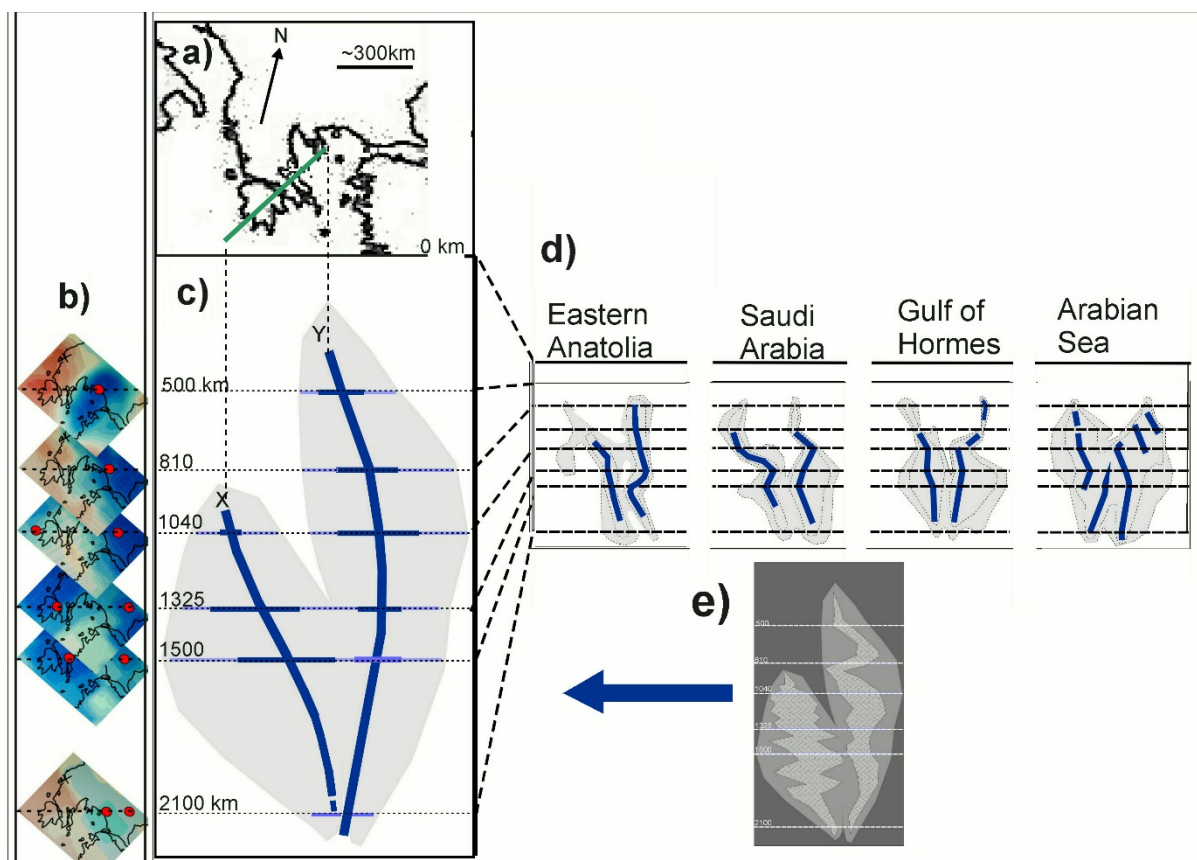
103

104 with Schmid et al. (2020) that “Vardar zone” (Fig. 2b) is not synonymous  
 105 with “Vardar ocean”. In our opinion, the Vardar zone is not the “root” “of  
 106 Vardar-derived thrust sheets, as has been often suggested (Zimmerman  
 107 and Ross 1976; Brown and Robertson 2004; Froitzheim et al. 2014).  
 108 Quite the contrary, as will be shown, the “Vardar zone” is where the last  
 109 slab of the Vardar ocean subducted (Scherreiks and BouDagher-Fadel  
 110 2020a and 2020b) and probably corresponds to the “Sava suture zone”  
 111 (Ustaszewski et al. 2010; Schmid et al. 2020).

112 The names of geo-tectonic sub-divisions of the Vardar zone used herein  
 113 are after Kockel (1979).

114 The “Vardar zone” corresponds to the northwest-southeast striking belt  
 115 (Fig. 1a) where remnants of island arc volcanic formations are found  
 116 (Mercier, 1968; BeBien et al. 1994; Brown & Robertson 1994; Mercier  
 117 and Vergely, 2002; Saccani et al. 2008; Sharp and Robertson 2006;  
 118 Katrivanos 2013) and where easternmost Pelagonia is covered by Upper  
 119 Cretaceous carbonates (Schmid et al. 2020).

120 We consider it important to use the term “ophiolite,” in the strict sense of  
 121 the “Steinmann Trinity” (Bernoulli et al.), because there are oceanic  
 122 formations in the study areas that although they are composed of basalt  
 123 +- radiolarite they are devoid of serpentinite and had been derived from  
 124 tectonic environments unrelated to obduction, which will be shown.  
 125 Furthermore, the term “mélange”, used herein, follows Hsü (1974)  
 126 referring to tectonically produced polymictic fault-zone rocks as opposed  
 127 to polymictic sedimentary deposits (see also Scherreiks 2000). The  
 128 mélanges are associated with mylonitic S-C shear fabrics of subduction  
 129 zones (Meneghini et al. 2009) like those found in the Vardar zone  
 130 (Katrivanos et al. 2013).  
 131



132  
 133 Fig. 3 (see figure captions)  
 134

135 ***The carbonate platforms of Adria and the Vardar zone***

136 Following the afore said and our own research, Adria was the pedestal  
 137 of a vast subsiding carbonate platform, of the marginal, foreland  
 138 category (Kendall and Schlager 1981; Schlager 2000; Bosence 2005)  
 139 that extended from the Alps (Fruth and Scherreiks 1982, Bosellini 1984)  
 140 through Korab-Pelagonia and into the west Taurides (Flügel 1974,1983;  
 141 Scherreiks 2000) (Fig. 1, Fig. 2b) and across the western Tethys  
 142 (BouDagher-Fadel and Bosence 2007). The platform evolved adjacent  
 143 to the west side of the Vardar ocean during the Late Triassic through the

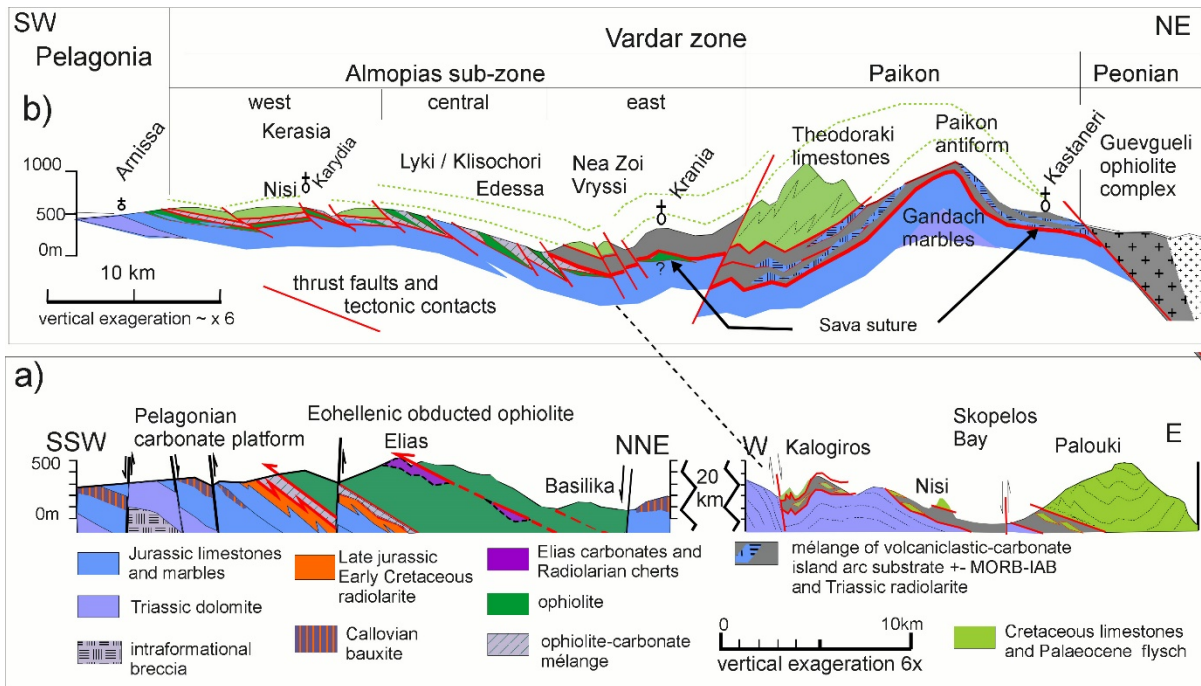
144 Early Jurassic from a cyclically alternating supratidal to a peritidal  
145 domain (Scherreiks 2000; Bosence et al. 2009) and then responded with  
146 subsidence and episodes of upheaval as continental Adria and the  
147 Vardar ocean converged (Scherreiks et al. 2010, 2014, 2016). (Table 1a  
148 documents biostratigraphic data concerning the Pelagonian carbonate  
149 platform of Evvoia and the Northern Sporades, which will be referred to  
150 in the text.)

151 In the Vardar zone at the east side of the Vardar ocean (Fig. 2b) one  
152 finds the remnants of a carbonate platform that evolved during the  
153 Cretaceous, most probably on the forearc margin of the Vardar arc  
154 (Fig.2b) whose evolution terminated during the Paleocene (Mercier  
155 1968; Mercier and Vergely 2002). The inevitable crash between  
156 Pelagonia and the Vardar zone (Fig.2b) was a crash between two  
157 Cretaceous platforms (see Discussion). (Significant biostratigraphic data  
158 concerning carbonate platform of the Vardar zone are documented in  
159 Tables 1b and 1c and will referred to).

160

### 161 ***The Pelagonian carbonate platform and its involvement in the*** 162 ***demise of the Vardar ocean***

163 The Vardar ocean existed during the Middle to Late Triassic,  
164 substantiated by radiolarians and pillow basalt found in ophiolite  
165 occurrences in our study area in Evvoia (Danelian and Robertson 2001;  
166 Chiari and Marcucci 2003; Gings and Schauer 2005; Gawlick et al.  
167 2008; Scherreiks et al. 2010; Chiari et al. 2012) (Table 1a11.1). Initially,  
168 the Late Triassic and Early Jurassic carbonate platform evolved from a  
169 cyclically alternating supratidal to peritidal domain (Scherreiks 2000;  
170 Bosence et al. 2009) and then began sinking, presumably responding  
171 with subsidence as Adria converged with the Vardar oceanic plate  
172 (Scherreiks et al. 2010). The postulated beginning of Intra-oceanic  
173 obduction was around Toarcian to Bajocian time (180–170 Ma), based  
174 on the ages of amphibolites found in the “metamorphic sole” of  
175 subduction-zone mélanges (Roddick et al. 1979; Spray and Roddick  
176 1980; Spray et al. 1984). The platform subsided during the Middle  
177 Jurassic, verified by ever deepening carbonate facies (Scherreiks 2000),  
178 and then became emergent during Callovian time, verified by bauxite  
179 deposits (Fig. 4a) (Scherreiks et al. 2016). The age of this Callovian  
180 upheaval has been verified with Bathonian foraminifera in the limestones  
181 below, and Oxfordian foraminifera above the bauxite crusts (Table 1a 5  
182 and 6) (ibid.). The “Callovian event” has been attributed to plate tectonic  
183 stress that affected the entire Mediterranean region (Meléndez et al.  
184 2007). An Oxfordian transgression re-established shallow marine  
185 environments which generated a Tethys-wide reef facies that extended  
186 from the Alps to Asia and in the Hellenides is characterised by the



188

189 Fig. 4 (see figure captions)

190

191 demosponge, *Cladocoropsis mirabilis* Felix (Flügel 1974; Scherreiks  
 192 2000) (Table 1a 7 and 8). Rapid platform subsidence and drowning  
 193 below the CCD occurred during Tithonian-Berriasian time, verified by  
 194 radiolarian cherts (Baumgartner and Bernoulli, 1976). The final ophiolite  
 195 emplacement is estimated to have occurred in Valanginian time, in  
 196 Evvoia, after flysch-like sedimentation had been shut off by the  
 197 obduction (Scherreiks 2000; Scherreiks et al. 2010; Scherreiks et al.  
 198 2014). The obduction was followed by a period of ophiolite erosion and a  
 199 subsequent gradual, widespread, transgression of marine conglomerate  
 200 in Evvoia and across the Pelagonian zone during Early cretaceous time  
 201 (Scherreiks 2000; Fazzuoli et al. 2008; Photiades et al. 2018) (Table 1a  
 202 9).

203

### 204 ***Palaeogeography of the Vardar ocean decerned from seismic*** 205 ***tomographic images of the mantle below the Hellenides***

206 Seismic tomographic images of the Alpine-Himalayan realm (BSE  
 207 models, Bijwaard et al. 1998) depict mantle-perturbations of subducted  
 208 slabs of Neotethys oceanic lithosphere (Bijwaard and Spakman 2000;  
 209 Hafkenscheid 2004; van der Meer et al. 2018).

210 Van Hinsbergen and others (2005) recognised two separate and distinct  
 211 perturbations in tomographic images as probable Neotethys slabs.

212 For our investigations, we have enlarged the tomographic images of the  
 213 areas below the Hellenides and have decerned that there are two slabs  
 214 (Fig. 3a-c). To check this out, we looked further eastwards to the

215 Arabian Sea (Fig. 3d) and have corroborated that two slabs of oceanic  
216 lithosphere have subducted there also. We have interpreted the  
217 perturbations beneath Hellenides as sunken Vardar ocean lithosphere  
218 and are of the opinion that the images verify two episodes of subduction  
219 (Scherreiks and BouDagher-Fadel 2020a) (Fig. 3c) (see Discussion and  
220 conclusions).

221

## 222 **The study areas**

223

### 224 ***Evvoia and Northern Sporades***

#### 225 ***Ophiolites and Platforms***

226 Examples of obducted ophiolite s. str. occur in the study areas of  
227 northern Evvoia (Fig. 4a) (Scherreiks 2000; Scherreiks et al. 2014) and  
228 are found throughout the Korab-Pelagonian zone (Fig. 1). They lie,  
229 tectonically emplaced, together with mélangé on top of Upper Jurassic  
230 and Lower Cretaceous carbonate platform rocks (Jacobshagen et al.  
231 1976; Jacobshagen 1986). The ophiolites are erosional remnants that  
232 have been postulated to be parts of a single obducted ophiolite sheet  
233 that was emplaced during the Late Jurassic to Early Cretaceous, an age  
234 which classifies it as “Eohellenic” after Jacobshagen et al. (1976). The  
235 onetime ophiolite sheet is considered to have had a width of at least  
236 200km - when judged from the width of the ophiolite outcrops on  
237 geologic maps (Gawlick et al. 2008; Schmid et al., 2020) (Fig. 1).

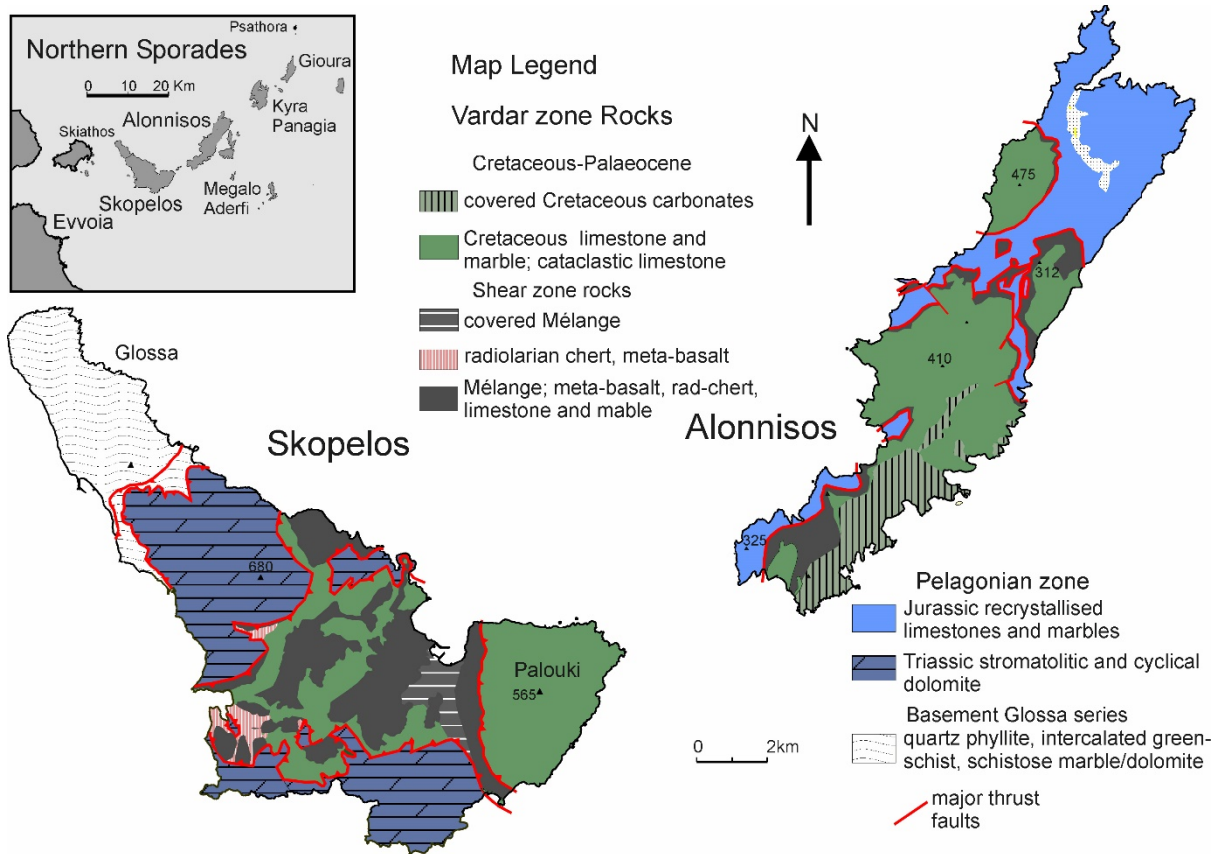
238

239 The Northern Sporades are devoid of serpentinite. The ophiolite sheet  
240 including large parts of the Pelagonian substrate had been removed by  
241 erosion during Early Cretaceous time (Fig. 5). The eroded surface of  
242 Jurassic and Triassic platform carbonates is covered by a sheet of  
243 mélangé composed of meta-basalt and radiolarian chert which is  
244 chaotically mixed with carbonate breccia and mylonitic phyllonites  
245 (Scherreiks and BouDagher-Fadel 2020a) (Fig. 4a and Fig. 5). Slices of  
246 Cretaceous and Paleocene platform carbonates of reefal origins are  
247 tectonically incorporated in the mélangé (Table 1a 10-10.3). The  
248 Cretaceous carbonate platform successions of Alonnisos and Skopelos  
249 overlie the mélangé. In corroboration with Kelepertsis (1974) we suggest  
250 that the Cretaceous and Paleocene carbonates of the northern  
251 Sporades are of Vardar zone origin, which will be expanded upon in the  
252 Discussion and Conclusions. The Cretaceous carbonate platform and its  
253 mélangé substrate, we suggest, correlate with an analogically similar  
254 succession in the Almopias sub-zone (Fig. 4a-b).

255

256

257



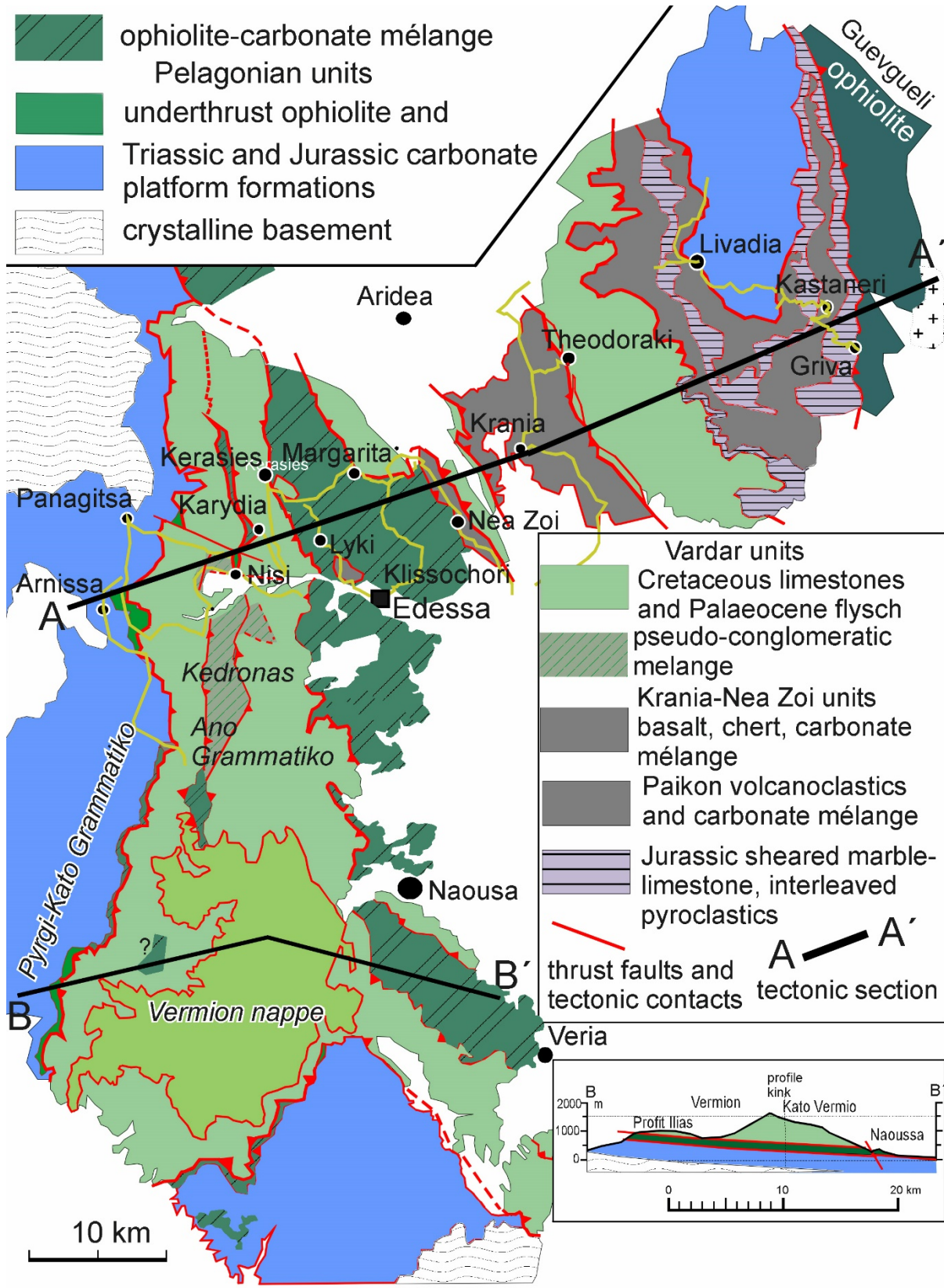
259  
260 Fig. 5 (see figure captions)

261

## 262 **The Vardar zone**

### 263 **West Almopias and its tectonic contact with Pelagonia**

264 Sheared Eohellenic ophiolite occurs on top of Pelagonian carbonates in  
 265 contact with disrupted Cretaceous limestones (Table 1b 1 and 2), along  
 266 the western border of the Vardar zone, for example near Panagitsa and  
 267 Arnissa Fig. 6) (Mercier and Vergely 1988) and southwards near Pyrgi-  
 268 Kato Grammatiko and west of the Vermion mountains (Georgiadis et al.  
 269 2016) (Fig. 6). West verging imbricated thrust faults characterise this  
 270 western boundary of the Vardar zone, from the Dinarides through the  
 271 Hellenides (in Jacobshagen (1986) from Mercier (1973), Mercier and  
 272 Vergely (1979)). The base of the imbricates is Eohellenic ophiolite and  
 273 the Triassic-Jurassic carbonate platform of the Pelagonian zone which is  
 274 covered by disrupted ophiolite followed by schistose pyroclastic units  
 275 interleaved with slices of radiolarian cherts, volcanoclastic and chloritic  
 276 marble layers. This tectonic transition between Pelagonia and the  
 277 western edge of the Vardar zone is shown by Sharp and Robertson  
 278 (2006) in the Arnissa area (Fig. 6): a ~500-metre-thick succession of  
 279 imbricated ophiolite mélangé. This succession is topped off by limestone  
 280 debris with Rudists and Planktonic foraminifera, *Globo truncana* (Mercier  
 281 and Vergely 1988) (Table 1b 3) (Plate 1). In agreement with these



283 Fig. 6 (see figure captions)

284 observations, we underscore that the contact between the Vardar and

285 Pelagonian zone is a thrust-fault-zone (see Discussion). Although

286

287

288 Cretaceous carbonates have been supposed to *transgressively* overlie  
289 laterite and serpentinite (Mercier and Vergely 1988; Sharp and  
290 Robertson 2006; Photiades et al. 2018), we are of the opinion that the  
291 inferred transgressional conglomerates are cataclasites (Plate 2a-b) and  
292 that orthoconglomerates (Friedman 2003) that could substantiate a  
293 marine transgression have not been verified (see Discussion and  
294 conclusions). Furthermore, the Cretaceous limestones of the Vardar  
295 zone are in tectonic contact with the subjacent ophiolite even where  
296 laterite is found at the contacts. The circumstances here are analogical  
297 to the Northern Sporades where a *sedimentary* contact of the  
298 Cretaceous Carbonates with its original substrate is nowhere to be found  
299 (Scherreiks and BouDagher-Fadel 2020a).

300

### 301 ***Tectonic windows in west Almopias***

302 Serpentinite and ophiolite-carbonate mélangé crop out, as tectonic  
303 windows, through the Cretaceous limestone cover along a narrow,  
304 elongated zone of north-south striking faults, extending from Kerassia-  
305 Karydia-Kedronas (Mercier and Vergely 1972; 1988) and to Ano  
306 Grammatiko (Sacciani et al. 2008; Georgiadis et al. 2016) (Fig. 6).  
307 Extensive exposures consist of “conglomeratic” rocks (Mercier and  
308 Vergely 1988), which in our opinion are cataclasites (see Discussion).  
309 The “conglomeratic” rocks contain Triassic and Jurassic carbonates as  
310 well as limestones ranging in age from Cenomanian to Turonian (Table  
311 1b2) and overlie Pelagonian serpentinite (ibid.). Near Nisi and Karydia  
312 (Fig. 6) these cataclasites (Plate 2a-b) occur below Campanian  
313 limestone (Table 1b 4) (Plate 1). At its base, this succession contains  
314 olistolith marbles of Triassic-Jurassic age and overlie white micaceous  
315 Triassic marbles in suggested *transgressional* contact (ibid). We dispute  
316 a transgressional origin of the Kedronas-Nisi “conglomerate” (see  
317 discussion on pseudo-conglomerates). The tectonic windows exposing  
318 underthrust Pelagonian ophiolite rocks can be followed in west Almopias  
319 from the north near Karydia to the Vermion area (Georgiadis et al.,  
320 2016) (Fig. 6, see section B-B’).

321

### 322 ***Pelagonian ophiolite exposures of central Almopias***

323 An extensive imbricated belt of ophiolite mélangé some 50 kilometres  
324 long and 5-10 kilometres wide can be traced from the Lyki-Klissochori  
325 area (Mercier and Vergely 1984; 1988) to the Naousa and Veria areas  
326 (Fig. 6) (Saccani et al. 2008; 2015; Georgiadis et al. 2016). The mélangé  
327 is interleaved with slices of marble and Jurassic carbonates, which we  
328 agree, are of Korab-Pelagonia origin (Bortolotti et al 2013; Georgiadis et  
329 al. 2016) (Table 1b 6 and 7-7.2). The carbonates contain an Oxfordian-  
330 Kimmeridgian reefal fauna, including *Cladocoropsis* sp. of Late Jurassic

331 age (Mercier and Vergely 1984). As pointed out above, this is a typical  
332 Kimmeridgian-Tithonian reef facies of the Pelagonian zone (Scherreiks  
333 2000) (Table 1a 7-8) that had been overthrust by Eohellenic ophiolite  
334 during the Early Cretaceous. In the Vardar zone, the Pelagonian  
335 ophiolites are locally interleaved with sericitized basalt schist (Lyki) (see  
336 Geochemistry) and are in underthrust position beneath “conglomeratic”,  
337 ophiolitic mélange and upper Cretaceous carbonates (north-east of  
338 Margarita, Fig. 6) (Table 1b 7).

339 In accord with the afore cited researchers and the described geology, we  
340 support the opinion that the ophiolites and Upper Jurassic carbonates  
341 found in the west and central Vardar sub-zones are tectonically inherited  
342 from underthrust Pelagonia (Fig. 4b).

343

### 344 ***Eastern Almopias and Paikon units***

345 A noteworthy difference between the eastern and western units of the  
346 Vardar zone is that the eastern Almopias and the Paikon units are  
347 devoid of serpentinite which we corroborate from Tranos et al., 2007.  
348 Serpentinite, however, probably exists at depth but is not exposed (Fig.  
349 4b), as it is further north in an area known as Ano Garefi, where  
350 serpentinitized peridotite is exposed below basalt (saccani et al. 2015).  
351 The mélanges of the Nea zoi-Vryssi-Meglenitsa and Krania units (Fig. 4b  
352 and Fig. 6) are composed of dolerite, pillow basalt and tuff and contain  
353 upper Jurassic-lower Cretaceous radiolarite (Mercier and Vergely 1984),  
354 with a relict Cretaceous cover (Table 1c 1.-1.2). Slices of Triassic lavas  
355 and radiolarites (Stais et al. 1990) (Table 1c 3 and 4) and upper  
356 Cretaceous arenites are also incorporated into the foliated matrix of the  
357 mélange of the Krania-Vryssi units (Saccani et al. 2015). The “*ophiolite*  
358 *related*” mafic units, “*ophiolite nappe*” and “*Meglenitsa Ophiolite*”,  
359 reported as ophiolite in Sharp and Robertson 2006 (from Sharp 1994  
360 and Sharp & Robertson 1998) in our opinion are not ophiolites s. str. but  
361 consist of ocean floor or arc basaltic rocks (see Geochemistry).

362

### 363 ***The Paikon antiform, a Pelagonian window: Katrivanos et al. 2013***

364 The Theodoraki limestone is the youngest formation of the Paikon  
365 antiform (Katrivanos et al. 2013). The limestone is part of the  
366 Cretaceous carbonate platform that covers the entire Vardar zone, and  
367 which is composed of a wide range of neritic to reefal facies (Table 1b  
368 and Table 1c Theodoraki unit). The platform is in tectonic contact with a  
369 pile-up of SW dipping slices of Theodoraki limestones and slices of  
370 volcano-sedimentary rocks including radiolarites, tuffites and lava, and  
371 Triassic-Jurassic Marble and schist of Pelagonian origin (Mercier and  
372 Vergely 2002). Katrivanos and others (2013) corroborate that the  
373 tectono-stratigraphic sequence is composed of volcano-clastic rocks

374 together with limestones of Middle to Late Jurassic age, based on micro  
375 and macro-faunas including *Cladocoropsis mirabilis* (Griva-Kastaneri  
376 formation Fig. 4b, Fig. 6) (Table 1c Griva-Khromni units). The volcano-  
377 sedimentary slices are on top of Triassic-Jurassic Gandatch marbles  
378 and schists (Fig. 6). All the volcanic material of this series is *strongly*  
379 *mylonitized in discrete, narrow shear zones* related to mylonitic foliation  
380 (Katrivanos et al. 2013). The carbonate rocks are mylonitized, near the  
381 contacts with tectonically overlying volcano-sedimentary slices e.g., at  
382 Kastaneri (ibid). Our investigations corroborate the above observations,  
383 which lead us to interpret the volcano-sedimentary formations in the  
384 substrate of the Theodoraki limestone as a composite allochthonous  
385 mélange complex in which slices of volcanic and sedimentary rock-units  
386 can be individually distinguished.

387 On the contrary to the above, the Paikon unit has been depicted (Sharp  
388 and Robertson 1994) to consist of a contiguous sedimentary,  
389 stratigraphic, succession extending from the Triassic to Cretaceous time  
390 only interrupted by an Oxfordian and Cenomanian unconformity, which  
391 we dispute.

392 We share the opinion that the Paikon is an antiform and a Pelagonian  
393 tectonic window (Katrivanos et al. 2013), and that the Paikon unit of the  
394 Vardar zone was most probably part of a volcanic island arc complex  
395 (Mercier et al. 1975; Mercier et al. 2002; BeBien et al. 1994; Brown &  
396 Robertson 2004; Mercier and Vergely 2002; Saccani et al. 2015, Schmid  
397 et al. 2020). Our envisioned island arc scenario, like others, evolved as  
398 the eastern Vardar ocean subducted north-eastwards beneath the  
399 margin of the European continent, which initiated subduction-related arc  
400 volcanism (Mercier and Vergely 2002; Brown and Robertson, 2004;  
401 Saccani et al., 2015). This was accompanied by back-arc spreading  
402 (Hafkinscheid, 2004; Schmid et al. 2020), represented by the Guevgueli  
403 ophiolite complex (Fig. 4b) (Anders et al. 2005; Saccanni et al. 2008b;  
404 Bortolotti et al. 2013; Michail et al. 2016).

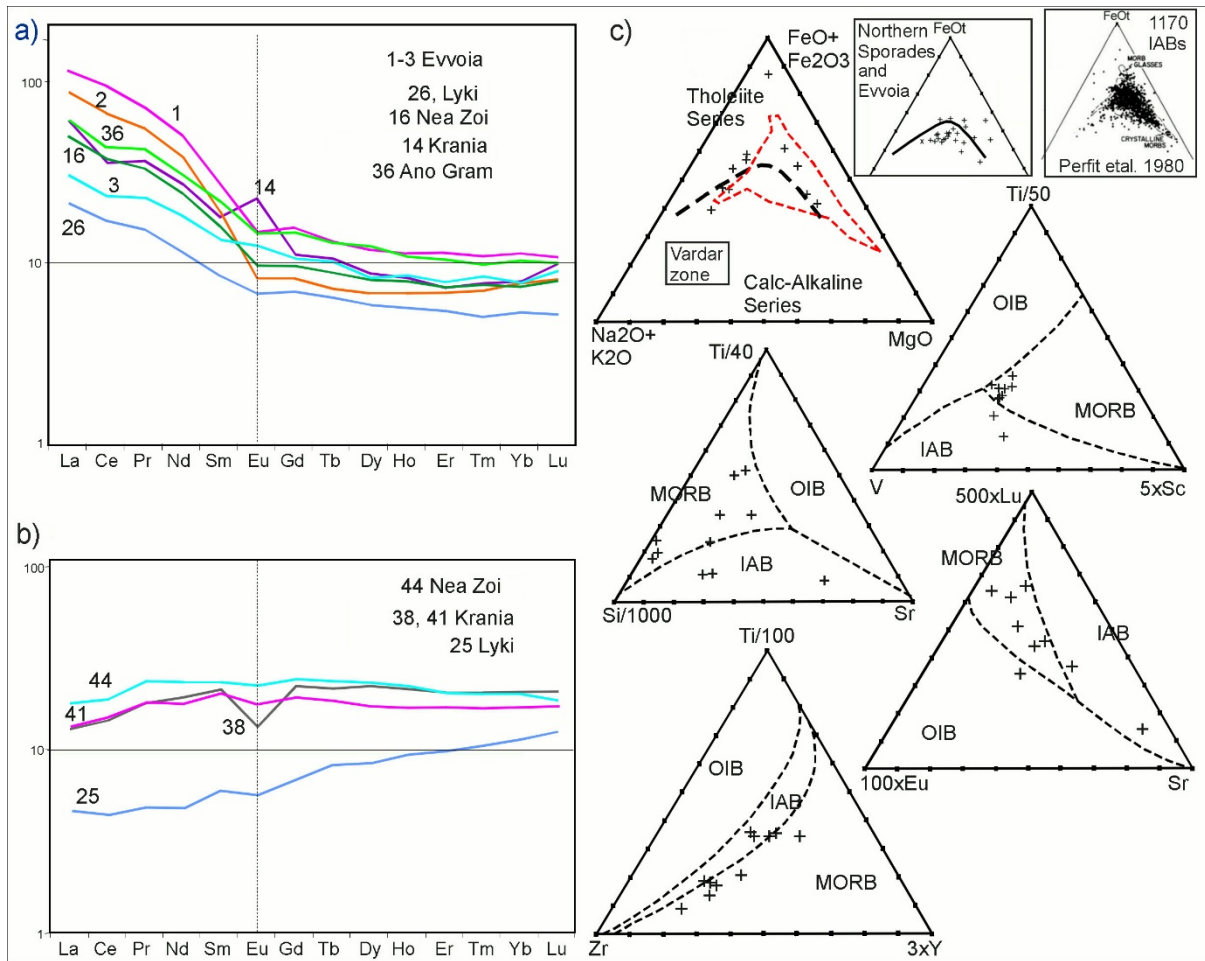
405

## 406 **Discussion and conclusions**

407

### 408 ***Geochemistry***

409 Meta-basalts from the Vardar zone and from northern Evvoia have been  
410 analysed for their major, minor and trace element contents, and some  
411 previous analyses are shown from the Northern Sporades (Scherreiks  
412 and BouDagher-Fadel 2020a). The analytical results are in Tables 2a  
413 and 2b. Rare-Earth (REE) plots and ternary discrimination diagrams  
414 (Fig. 7) have been drafted for the purpose of ascertaining basalt origins  
415 (after Pearce and Cann 1973; Perfit et al. 1980; Vermeesch P, 2006).



417

418 Fig. 7 (see figure captions)

419

420 Two serpentinized peridotites associated with basalts and radiolarian  
 421 cherts from Pelagonian ophiolites of Evvoia were previously analysed  
 422 (Scherreiks and BouDagher-Fadel 2020a) (Table 2b).

423 The meta-basalts of the Vardar zone and the Northern Sporades occur  
 424 in mélanges and they are sheared and sericitized and strongly  
 425 weathered, which may have caused contaminations with adjacent rocks,  
 426 making unambiguous differentiation between MORB and island IAB  
 427 additionally more enigmatic than it intrinsically is anyway (Perfit et al.  
 428 1980). None of the analyses (Table 2a) have abnormal Cr or Ni contents  
 429 which excludes serpentinite contamination (compare Cr and Ni Table 2b  
 430 samples 2-3).

431 The REE plots are typical for basalts (Pearce and Cann 1973; Kay and  
 432 Hubbard 1978; Perfit et al. 1980; Hooper and Hawkesworth 1993) (Fig,  
 433 6a and 6b), depicting light REE (LREE) enhancement associated with  
 434 IABs, and flat LREE-depleted patterns of probable MORB origin. An  
 435 almost identical array of REE plots have been ascertained for the

436 Northern Sporades where the present authors had drawn the conclusion  
437 that MORBs and IABs had been tectonically mixed in the mélanges of  
438 an extensive thrust-fault zone (Fig. 7) (Scherreiks and BouDagher-Fadel  
439 2020a). As in the Northern Sporades, the REE-plots drafted for the  
440 Vardar zone indicate the side by side presence of both IAB and MORB  
441 (Fig. 7a-b). Discrimination diagrams (Fig. 7c) also indicate the  
442 ambiguous situation of determining that MORBs for samples in one  
443 diagram correspond to IABs in another. Following Perfit and others  
444 (1980) we have additionally checked out that according to Perfit (ibid)  
445 there are distinguishing differences in potassium, titanium, and total iron  
446 wt.% concentrations in IABs and MORBs: MORBs having  $<0.25$  K<sub>2</sub>O,  
447 IAB having  $>0.25$  K<sub>2</sub>O; IAB having  $<1.2$  TiO<sub>2</sub>, and  $>6-15$  total Fe. The  
448 results of this query, using data from tables 2a and 2b, it appears that  
449 most of our samples are IABs but there are numerous ambiguities  
450 which, presumably, are caused by tectonic mélange mixing.  
451 The analyses of the basalts from the Eohellenic ophiolite of Evvoia and  
452 those of the Elias complex are incorporated in the REE and AFM  
453 diagrams (Fig. 7a and c) (Table 2b) and they indicate MORB and IAB  
454 affinities.

455

### 456 ***The composite tectono-Stratigraphy of eastern Pelagonia and the*** 457 ***Vardar zone in context with the afore related geology***

458 Pelagonia consists of a Palaeozoic-Middle Triassic basement covered  
459 by a carbonate platform over which a 200 km-wide ophiolite sheet of  
460 west Vardar ocean lithosphere, had been obducted (Fig. 8a, b, c). The  
461 1700 km-wide eastern Vardar ocean subducted beneath the Vardar  
462 zone (vz) during Late Jurassic through Cretaceous time (Fig. 8c). Figure  
463 8a - b indicates that Pelagonia together with obducted Eohellenic  
464 ophiolite crashed with the Vardar zone and underthrust the Cretaceous-  
465 carbonate-platform and its volcano-sedimentary substrate (Fig. 8 b). As  
466 Pelagonia continued to advance it underthrust the Guevgueli complex  
467 and crashed with Serbo-Macedonia (Fig. 8b, c).

468

### 469 ***Major deformations***

470 Three major episodes of tectonic deformation, D1-D3, affected the  
471 Pelagonian and Vardar zones; each dominated by a major time-  
472 transgressive thrust fault complex (Fig. 8a-b). (Our D1-D3 indices do not  
473 correspond with those of previous researchers (Mercier and Vergely  
474 2002; Kiliyas et al. 2010; Katrivanos et al. 2013).

475



486 Cretaceous carbonate platform including its volcano-sedimentary  
487 substrate. Greenschist and HP/LT metamorphism described by  
488 Katrivanous et al. 2013 can be attributed to D2.  
489 Deformation D3 corresponds to the compression caused by the crash of  
490 the Pelagonian plate with Serbo-Macedonia, which caused folding in the  
491 Vardar and Pelagonian zones of which the Paikon antiform is the most  
492 prominent (Fig. 8b). Subsequently, shear-stress produced the youngest  
493 thrust faults in the flanks of the Paikon antiform (D3 in Fig. 8b) and most  
494 probably rejuvenated older faults, including numerous subordinate  
495 imbrication thrusts (Fig. 4b), described in Mercier and Vergely (2002),  
496 Kiliyas et al. (2010) and Katrivanos et al. (2013).

497

### 498 ***Pseudo conglomeratic mélange of Kedronas, Nisi and Karydia***

499 The breccio-conglomeratic, cataclastic rock complex that contains  
500 abundant rounded clasts occurs incorporated in an extensive fault zone  
501 mélange in the west Almopias unit between Karydia and Ano  
502 Grammatiko (Plate 2a-b) (Fig. 6 pseudo conglomeratic mélange). In the  
503 Nisi-Karydia area the cataclasites are in tectonic contact with  
504 Campanian limestones (Plate 1) (Table 1b 4.1) on top and Pelagonian  
505 ophiolite at the base. We regard the cataclasites as matrix supported  
506 parabreccias composed of poorly sorted >2mm, rounded to angular  
507 clasts (Plate 2a-b). The clasts either consist predominantly of marbles,  
508 elongated pieces of sericitic calc-schists and dark micritic limestones  
509 (Plate 2b) or are chaotic mixtures of carbonate and ophiolite clasts  
510 (Plate 2a). Viewed under the microscope, the matrix is a chaotic breccia  
511 of calcitic grains that are not bound by interstitial pore cement (Bathurst  
512 1976) but by insular patches of aggrading neomorphic sparry calcites  
513 that had grown amid the much smaller angular granules of the matrix  
514 (Plate 2c, d, e). Crushed neomorphic calcite occurs in the matrix  
515 inherited from earlier stages of shearing. The neomorphic calcite, unlike  
516 cement, exhibits irregular boundaries and palimpsest, relic-matrix texture  
517 (Plate 2 d-e). The neomorphic calcites exhibit residual stress, indicated  
518 by crossing twins, stopping twins, twin thickening, and bending, which  
519 appears in low temperature stress regimes below 200 °C. (Burkhard  
520 1993; Chen et al, 2011). Neomorphism had most likely taken place in a  
521 dry sub-metamorphic environment (Folk 1965 in Bathurst 1976).  
522 It is suggested that the larger components underwent rounding and  
523 grain-reduction by granulation from the decimetre to centimetre scale to  
524 microscopic micron scale, which is not unusual in tectonic breccias in

525 which the fragments may be worn down and rounded by tectonic  
526 grinding (Norton 1917; Higgins 1971; Woodcock and Mort 2008).  
527 We dispute that this rock complex had a transgressional origin (Mercier  
528 and Vergely 1988; and Mercier 1966 in Sharp and Robertson 2006)  
529 because it does not display the most important characteristics that  
530 marine conglomerates should have: clast-clast support and diagenetic  
531 cement (Bathurst 1976; Friedman 2006). On the contrary the clasts are  
532 matrix supported and the grains have not been diagenetically cemented.  
533 In our opinion the “parabreccio-conglomerate” formed as Pelagonia  
534 underthrust the Vardar zone during Paleocene time (D2 above).

535

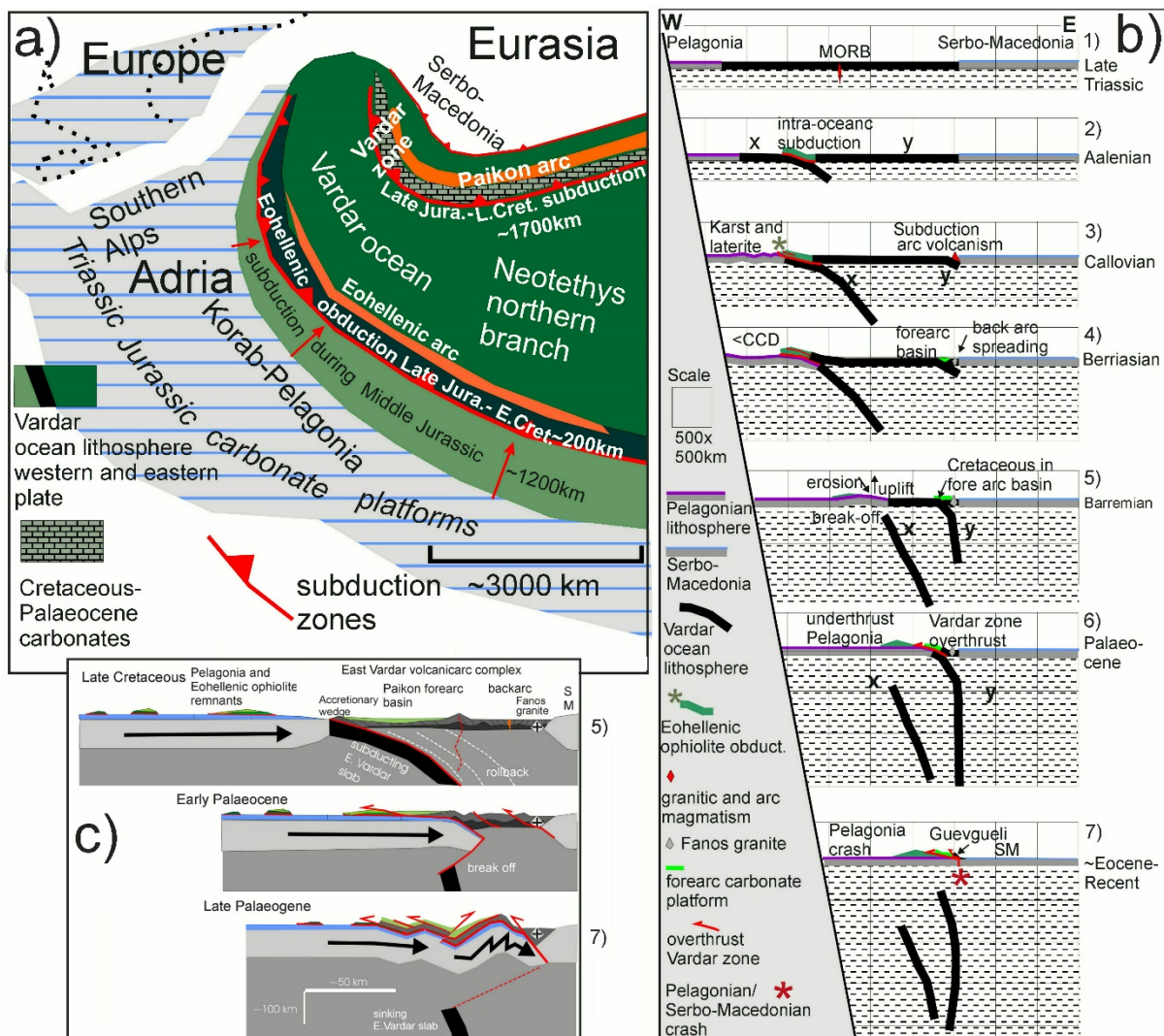
### 536 **The crash of two Cretaceous carbonate platforms**

537 It should be taken into consideration that some remnants of the well  
538 documented Cretaceous Pelagonian carbonate platform (Fig. 8a), may  
539 have been subducted (“piggy-backed”) beneath the Cretaceous  
540 carbonate platform of west Almopias, at the latest during Paleocene  
541 time, and thus inherited Pelagonian-orthoconglomerates could occur in  
542 the mélanges beneath the Vardar zone (e.g., Vermion: Photiades et al.  
543 2018).

544

### 545 **New Palaeogeography**

546 From the previous chapters and from seismic tomography it is  
547 postulated that the Vardar ocean subducted along two subduction zones  
548 (Fig. 9a). The western intra-oceanic subduction zone evolved about  
549 Toarcian to Aalenian time, based on radiometric ages of amphibolites in  
550 sub-ophiolite mélanges, and continued to subduct through the Middle  
551 Jurassic verified by late Middle Jurassic radiolarians in the sub-ophiolite  
552 mélange in Evvoia (Danelian and Robertson 2001; Higgins and  
553 Schauer 2005 (Scherreiks et al. 2014) (Table 1a 11.2 and 12). A supra-  
554 subduction volcanic arc evolved during the Middle Jurassic, documented  
555 by the Elias complex of northern Evvoia (Fig. 4a) which presumably was  
556 part of a more extensive supra-subduction “Eohellenic arc” (Fig. 9a)  
557 (ibid.). The beginning of the Eohellenic obduction, is suggested to have  
558 begun during Bathonian time together with the Callovian upheaval  
559 (Meléndez et al. 2007) and the eastward subduction of the eastern  
560 Vardar ocean (Fig. 9b3). The Vardar, supra-subduction, volcanic island  
561 arc and the spreading Guevgueli back arc ophiolite complex evolved  
562 during (Middle?) Late Jurassic and Cretaceous time. We envisage a  
563 Paikon forearc basin, rimmed by an accretionary wedge like that shown  
564 in Sacconi et al. (2008b) in which the basin floor was covered by



566

567 Fig. 9 (see figure captions)

568

569 (volcanoclastic) basalt without carbonates during the lower Middle  
 570 Jurassic. To our knowledge, a Jurassic carbonate platform did not  
 571 evolve on the east side of the Vardar ocean. Instead, we suggest that  
 572 volcanoclastic deposits accumulated on the flanks of the Vardar volcanic  
 573 arc and became the substrate of carbonate accumulation beginning in  
 574 Aptian time. Investigations of the Guevgueli back arc basin have not  
 575 disclosed relicts of a Mesozoic carbonate platform (Saccani et al.  
 576 2008b).

577

578 **The Cretaceous forearc carbonate platform of the Vardar zone**

579 The Cretaceous Vardar-zone carbonate platform is envisaged to have  
 580 evolved over the late Jurassic-early Cretaceous volcanoclastic substrate  
 581 of the forearc basin (Fig. 9a) (Saccanni et al. 2008b).

582 The earliest recorded Cretaceous limestones in the Vardar zone are of  
583 Aptian age (Table 1b4.2, Table 1c6.1). The bio facies indicate a reefal to  
584 inner neritic environment having had depths of between 10 and 50m  
585 (BouDagher-Fadel 2018a). These limestones are in the west Almopias  
586 sub-zone (Fig. 4b) and may have been deposited near or on the  
587 accretionary wedge of the forearc basin (Sacconi et al. 2008b). The  
588 verified bio facies indicate that patch reef and neritic environments  
589 existed side by side through Cenomanian, Santonian, Campanian, and  
590 Maastrichtian time (Table 1b West Almopias) (Plate 1). The deeper  
591 neritic platform facies occur eastwards in the central and east Almopias  
592 sub zones, ranging in age from the Cenomanian to Maastrichtian (Table  
593 1b-c Central and East Almopias). The bio stratigraphic succession in the  
594 Theodoraki limestone formation begins with Cenomanian/Turonian reef  
595 facies that may represent a fringing reef along the outer slopes of the  
596 arc. Inner neritic facies deepen upwards, from the Campanian to  
597 Maastrichtian times (Table 1c 5 Theodoraki unit). Late Maastrichtian  
598 flysch signals the demise of the Cretaceous carbonate platform of the  
599 Vardar zone.

600 From the afore said, a tentative picture of the platform-architecture can  
601 be discerned: it was a subsiding environment in which about 500 m of  
602 carbonates accumulated (“carbonate factory” Schlager 2000) during  
603 about 60Ma between Aptian and Maastrichtian time (Mercier and  
604 Vergely 1984, 1988). Reefs evolved during Early Cretaceous along an  
605 outer western accretionary wedge and inner eastern high where fringing  
606 reefs on the outer slopes of the Paikon volcanic arc interdigitated outer  
607 neritic carbonate facies in the central basin.

608

### 609 **Seismic tomographic images of the mantle below the Hellenides**

610 We have interpreted the perturbations beneath Hellenides as sunken  
611 Vardar ocean lithosphere and are of the opinion that the images verify  
612 two episodes of subduction (Scherreiks and BouDagher-Fadel 2020a)  
613 (Fig. 3c).

614 The vertical section (Fig. 3c) shows that the leading edges of each slab  
615 has subsided to a depth of about 2000 kilometres. Presently, the trailing  
616 edge of the western slab (x in Fig. 3c) is about 900 kilometres below the  
617 Earth’s surface and the trailing edge of slab (y) is about 400 kilometres  
618 below the surface. These are the depths to which the slabs have sunken  
619 since their breakoffs. In estimating the width of a slab, however, one  
620 must consider that a subsiding lithospheric plate certainly undergoes  
621 compression and deformation which can make width-estimates

622 inaccurate (Fig 3e). The seismic tomographic images are, nevertheless,  
623 presently the best possible way to estimate the onetime width of the  
624 subducted oceanic lithosphere which we estimate to have been about  
625 3000 kilometres (determined by adding together the lengths of the slabs  
626  $(x + y) \sim 1200 + \sim 1700$  and adding, to that sum, the width of the  
627 obducted Eohellenic ophiolite sheet which has been assumed to be  
628 about  $\sim 200$  kilometres (Fig. 8c)). However, 3100km is the composite  
629 width, not necessarily the surface width that the Vardar ocean had at  
630 any one time. We do not know when the ocean ridge stopped spreading:  
631 subduction and ocean spreading at the ocean ridge could have taken  
632 place simultaneously.

633 The western slab (x) is supposed to have broken off and began sinking  
634 after the Eohellenic ophiolite had been emplaced during Valanginian  
635 time. The eastern Almopias slab (y) is supposed to have broken off after  
636 Pelagonia crashed and underthrust the Vardar-zone carbonate platform  
637 and volcanic arc complex.

638

### 639 ***Seismic tomographic model***

640 Our model (Fig. 9) postulates that the Vardar ocean was about 3000km  
641 wide and bordered on Adria in the west. This means that both the  
642 microplate Adria and the vaguely attached African plate, were situated  
643 3000km further southwest during Early Jurassic time as the Atlantic  
644 Ocean and the Alpine Tethys began spreading (e.g., Schmid et al. 2008;  
645 Scherreiks et al. 2010). This infers that Pelagonia, the eastern edge of  
646 Adria, moved about 3000km northeast towards the European continent  
647 (Fig. 9b) while the Atlantic spread.

648 The  $\sim 3000$ km wide Vardar ocean is supposed to have  
649 subducted/obducted, between  $\sim$ Sinemurian-Aalenian time ( $\sim 190$ - $175$   
650 Ma) and Paleocene time ( $\sim 65$  Ma), a timespan of  $190-65 = 125$  Ma;  $175-$   
651  $65 = 110$ Ma. Subduction rates of the oceanic slabs are estimated to  
652 range from about 3 cm/year ( $= 30\text{km}/1\text{Ma}$ ) in the upper mantle to about  
653 1 cm/year in the lower mantle (Norton 1999). Simple calculations show  
654 that at a rate of  $30\text{km}/1\text{Ma}$ , a  $3300\text{km}$  wide ocean would subduct in 110  
655 Ma; and a  $3000\text{km}$  wide ocean could subduct in 110Ma at a rate of  
656  $\sim 2.7\text{cm/a}$ .

657 In our example, we also consider that the trailing edge of Slab X sank  
658 900 km since breaking off after Valanginian time, and the trailing edge of  
659 slab Y sank about 400 km since its breakoff in the  $\sim$ Paleocene.

660 Sinking rates are lower in the mantle below 300–500 km, and in the  
661 lower mantle slab subsidence eventually approaches zero (Lallemand

662 and Funiciello 2009; Ichikawa et al. 2016). We have previously  
663 estimated (Scherreiks and BouDagher-Fadel 2020a. 2020b) that in using  
664 an average subsidence rate of 0.68 cm/year, one arrives at a  
665 Hauterivian break-off date for slab X (900km/6.8km/Ma ~132 Ma), and  
666 Late Paleocene as the break-off time of slab Y (400 km/6.8 km/Ma ~59  
667 Ma), which we believe corresponds to the known facts and is well in the  
668 range of plausibility.

669

## 670 **Summary**

671 The demise of the once over 3000-kilometre-wide Vardar ocean has  
672 been reconstructed from field investigations of its remnants in its  
673 onetime peripheries, and from seismic tomographic images of its  
674 remnants in the Mantle below the Central Hellenides. On its  
675 southwestern side the Vardar ocean bordered on the Pelagonian-  
676 Adriatic plate which was covered by a vast carbonate platform  
677 (BouDagher-Fadel and Bosence 2007) that evolved from a peritidal  
678 realm during Norian-Sinemurian- to a drowned platform during  
679 Tithonian-Berriasian-time. In the northeast the Vardar ocean bordered  
680 on Serbo-Macedonia of the European plate, where, during the Late  
681 Jurassic a supra-subduction volcanic island arc and back-arc complex  
682 emerged. A forearc reef and a shallow marine carbonate platform  
683 accumulated on top of a Jurassic-Early Cretaceous volcano-clastic  
684 substrate from about Aptian through Maastrichtian time.

685 The closure of the Vardar ocean occurred in one episode of ophiolite  
686 obduction and two episodes of intra-oceanic subduction.

- 687 1. During Middle Jurassic time a 1200-kilometre slab of west Vardar  
688 lithosphere subducted eastwards beneath the “Eohellenic”, arc,  
689 while a 200-kilometre-wide slab obducted westwards onto  
690 Pelagonia between Callovian and Valanginian time.
- 691 2. A 1700-kilometre-wide slab of east Vardar lithosphere subducted  
692 eastwards beneath the Vardar-zone arc-complex during Late  
693 Jurassic through Cretaceous time while Pelagonia underthrust the  
694 Cretaceous carbonate platform during the Paleocene.

695 In the greater framework of plate tectonics, the subduction of the Vardar  
696 ocean occurred simultaneously with the spreading of the Atlantic Ocean  
697 and the opening of the Alpine Tethys, while the Hellenides moved about  
698 3000 kilometres toward the northeast.

699 In the light of the present contribution, future research concerning the  
700 evolution of the Cretaceous carbonate platform of the Vardar zone could

701 advance our knowledge of the facies distributions and architecture of the  
702 Paikon fore arc basin. Another point of interest is the seismic  
703 tomography and the demise of the Guevgueli back arc since Paleocene  
704 time, which is also quite obscure.

## 705 **Acknowledgements**

706 *University College London:*

707 We are grateful to the Office of the Vice-Provost (Research, Innovation,  
708 and Global Engagement), especially Prof. David Price, for helping and  
709 facilitating our research.

710 The *Bayerische Staatssammlung für Palaeontologie und Geologie* in  
711 Munich, Germany, is thanked for their support during this research which  
712 is part of a 20-year research project. We thank ACTIVATION  
713 LABORATORIES LTD., Ancaster, Ontario, for carrying out the  
714 geochemical analyses. Special thanks are given Michael Born, Bonn,  
715 Germany for the preparation of thin sections.

716

## 717 **References**

718 Anders, B., Reischmann, T., Poller, U., Kostopoulos, D. (2005) Age and origin of  
719 granitic rocks of the eastern Vardar Zone, Greece: new constraints on the  
720 evolution of the Internal Hellenides. *J. Geol. Soc. London*, 162: 857-870.

721 Bathurst, R. G. C. (1976) Carbonate sediments and their Diagenesis. *Dev in*  
722 *Sedimentol* 12, Elsevier, 658pp

723 Baumgartner P. O., Bernoulli D. (1976) Stratigraphy and radiolarian fauna in a Late  
724 Jurassic–Early Cretaceous section near Achladi (Evvoia, Eastern Greece).  
725 *Ecl Geol Helv* 69:601–626

726 Baumgartner, P.O., Bartolini, A., Carter, E.S., Conti, M., Cortese, G., Danelian, T.,  
727 De Wever, P., Dumitrica, P., Dumitrica-Jud, R., Gorican, S., Guex, J., Hull,  
728 D.M., Kito, N., Marcucci, M., Matsuoka, A., Murchey, B., O'Dogherty, L.,  
729 Savary, J., Vishnevskaya, V., Widz, D. and Yao, A., (1995) Middle Jurassic to  
730 early cretaceous radiolarian biochronology of Tethys based on unitary  
731 associations. In: Baumgartner, P.O. et al., eds., Middle Jurassic to lower  
732 cretaceous Radiolaria of Tethys: occurrences, systematics, biochronology,  
733 *Mém. Géol.*, (Lausanne), 23, 1013-1048.

734 BeBien, J., Voet, P. B., Mercier, J. (1994): Geodynamic significance of the Paikon  
735 massif in the Hellenides: Contribution of the volcanic rock studies. *Bulletins of*  
736 *the Geological Society of Greece*, 30/1: 63-67.

737 Bernoulli, D., Manatschal, G., Desmurs, L., Müntener, O. (2003) Where did Gustav  
738 Steinmann see the trinity? Back to the roots of an Alpine ophiolite concept. in  
739 Dilek, Y., and Newcomb, S., eds., *Ophiolite concept and the evolution of*  
740 *geological thought: Boulder, Colorado, Geological Society of America Special*  
741 *Paper 373*, p. 93–110.

742 Bijwaard, H., Spakman, W. (2000) Non-linear global P-wave tomography by iterated  
743 linearized inversion. *Geophys. J. Int.* 141, 71-82

744 Bijwaard, H.W., Spakman, W., Engdahl, E.R. (1998) Closing the gap between  
745 regional and global travel time tomography. *J. Geophys. Res.*, 103, 30,055–  
746 30,078

747 Bortolotti, V., Chiari, M., Marroni, M., Pandolfi, L., Principi, G., Saccani, E. (2013)  
748 Geodynamic evolution of ophiolites from Albania and Greece (Dinaric-Hellenic  
749 belt): one, two, or more oceanic basins? *Int J Earth Sci* 102:783-811

750 Bosellini, A. (1984) Progradation geometries of carbonate platforms: examples from  
751 the Triassic of the Dolomites, northern Italy. *Sedimentology*, 31, 1-24

752 Bosence, D. (2005) A genetic classification of carbonate platforms based on their  
753 basinal and tectonic settings in the Cenozoic. *Sediment Geol* 175:49–72

754 Bosence, D., Procter, E., Aurell, M., Atef Bel, K., Boudagher-Fadel, M., Casaglia, F.,  
755 Cirilli, S., Mehdie, M., Nieto, L., Rey, J., Scherreiks, R., Soussi, M. and  
756 Waltham, D., (2009) A dominant tectonic signal in high-frequency, peritidal  
757 carbonate cycles? A regional analysis of Liassic platforms from western  
758 Tethys, *J. Sed. Res.*, 79(5-6), 389-415.

759 BouDagher-Fadel, M.K., Bosence, D.W.J. Early Jurassic benthic foraminiferal  
760 diversification and biozones in shallow-marine carbonates of western Tethys.  
761 *Senckenbergiana lethaea* 87, 1–39 (2007).

762 BouDagher-Fadel, M. K. (2008) The Mesozoic larger benthic foraminifera: the  
763 Jurassic. In: Boudagher-Fadel, M.K., ed., *Evolution and geological  
764 significance of larger benthic foraminifera*, Wignall PB (series ed) *Dev  
765 Palaeontol Strat* 21, Elsevier, Amsterdam.

766 BouDagher-Fadel, M.K., (2015) *Biostratigraphic and Geological Significance of  
767 Planktonic Foraminifera (Updated 2nd Edition)*. London: UCL Press.  
768 doi:10.14324/111.9781910634257.

769 BouDagher-Fadel, M.K. (2018a) *Evolution and Geological Significance of Larger  
770 Benthic Foraminifera*, Second ed. UCLPress, London. 704 pp.

771 BouDagher-Fadel MK. (2018) *Evolution and geological significance of larger benthic  
772 foraminifera*. London: UCL Press; 544pp

773 BouDagher-Fadel, M. K. (2018b) Revised diagnostic first and last occurrences of  
774 Mesozoic and Cenozoic planktonic foraminifera. UCL Office of the Vice-  
775 Provost Research, Professional Papers Series, 1-5.

776 BouDagher-Fadel, M., & Price, G. D. (2019) Global evolution and paleogeographic  
777 distribution of mid-Cretaceous orbitolinids. *UCL OPEN - ENVIRONMENT*.  
778 doi:10.14324/111.444/ucloe.000001

779 Brown, S., Robertson, A. (1994) New structural evidence from the Mesozoic-early  
780 Tertiary Paicon unit, Northern Greece. *Bull Geol Soc Greece*, 30/1: 159-170

781 Brown, S.A.M., Robertson, A.H.F. (2004) Evidence for Neotethys rooted within the  
782 Vardar suture zone from the Voras Massif, northernmost Greece.  
783 *Tectonophysics* 381, 143e173.

784 Burkhard, M. (1993) Deformation mechanisms and fabric Calcite twins, their  
785 geometry, appearance and significance as stress-strain markers and  
786 indicators of tectonic regime: a review. *Jour of Structural Geol*, 15, 3–5, 351-  
787 368

- 788 Chen, K., Kunz, M., Tamura, N. et al. (2011) Deformation twinning and residual  
789 stress in calcite studied with synchrotron polychromatic X-ray microdiffraction.  
790 *Phys Chem Minerals* 38, 491–500
- 791 Chiari, M., Marcucci, M. (2003) Triassic and Jurassic radiolarian assemblages from  
792 the siliceous sediments associated with pillow lavas in the Argolis Peninsula  
793 (Greece). *Abstr Tenth Meeting International Association Radiolarian*  
794 *Palaeontologists*, Lausanne: 40
- 795 Chiari, M., Bortolotti, V., Marcucci, M., Photiades, A., Principi, G., Saccani, E. (2012)  
796 Radiolarian biostratigraphy and geochemistry of the Koziakas massif  
797 ophiolites (Greece). *Bull. Soc. géol. France*, 183, no 4, 289-309.
- 798 Danelian, T., Robertson, A.H.F. (2001) Neotethyan evolution of eastern Greece  
799 Pagondas Mélange, Evia island inferred from radiolarian biostratigraphy and  
800 the geochemistry of associated extrusive rocks. *Geol Mag* 138:345–363
- 801 Fazzuoli, M., Menna, F., Nirta, G., Bortolotti, V., Carras, N., Principi, G. (2008) The  
802 Cretaceous transgression in the Dinaric-Hellenic orogen. *Soc. Geol. It.*, 6,  
803 *Nuova Serie*
- 804 Flügel, E. (1974) Fazies-Interpretation der Cladocoropsis-Kalke (Malm) auf  
805 Karaburun, W-Anatolien. *Arch Lagerstforsch (Ostalpen) Sonderbd 2*, Leoben,  
806 79-94
- 807 Flügel, E. (1983) Mikrofazies der Pantokrator-Kalke (Lias) von Korfu, Griechenland.  
808 *Facies* 8: 263-300
- 809 Friedman, G.M. (2003) Classification of sediments and sedimentary rocks. In Gerard  
810 V. Middleton, ed., pp. 127-135, *Encyclopedia of Sediments & Sedimentary*  
811 *Rocks*, *Encyclopedia of Earth Science Series*. Kluwer Academic Publishers,  
812 Boston, Massachusetts. 821 pp. ISBN 978-1-4020-0872-6
- 813 Froitzheim, N., Jahn-Awe, S., Frei, D., Wainwright, A.N., Maas, R., Georgiev, N.,  
814 Nagel, J.T., Pleuger, J. (2014) Age and composition of meta-ophiolite from the  
815 Rhodope Middle Allochthon (Satovcha, Bulgaria): a test for the maximum-  
816 allochthony hypothesis of the Hellenides. *Tectonics* 33(8):1477–1500
- 817 Fruth, I., Scherreiks, R. (1982) Hauptdolomit (Norian) – stratigraphy, paleogeography  
818 and diagenesis. *Sedimentary Geol*, 32: 195-231
- 819 Gallhofer, D., von Quadt, A., Schmid, S.M., Guillong, M., Peytcheva, I., Seghedi, I.  
820 (2017) Magmatic and tectonic history of Jurassic ophiolites and associated  
821 granitoids from the South Apuseni Mountains (Romania). *Swiss J. Geosci.*  
822 110, 699-719
- 823 Gawlick, H-J., Frisch, W., Hoxha, L., Dumitrica, P., Krystyn, L., Lein, R., Missoni, S.,  
824 Schlagintweit, F. (2008) Mirdita zone ophiolites and associated sediments in  
825 Albania reveal Neotethys ocean origin. *Int J Earth Sci (Geol Rundsch)*  
826 97:865–881
- 827 Georgiadis, G.A., Tranos, M.D., Kiliadis, A.A., Mountrakis, D.M. (2016) The  
828 emplacement of the Vermion nappe in the area of Kato Seli (Mt. Vermion  
829 Central Macedonia, Greece). *Bull. Geol. Soc. Greece*, vol. L, 24-33  
830 *Proceed. 14th Intern. Congr. Thessaloniki*
- 831 Gingins, Y., Schauner, O. (2005) Etude géochimique et paléontologique des  
832 séries Maliaques d'Othrys et du complexe d'Elias, Eubée du Nord, Grèce.  
833 *Diss Université de Lausanne*, Manuscript February 2005, 1–93pp

834 Hafkenscheid, E. (2004) Subduction of the Tethys Oceans reconstructed from plate  
835 kinematics and mantle tomography. Thesis, Faculty of Geosciences Utrecht  
836 University, The Netherlands. ISBN: 90-5744- 101-200.

837 Higgins, M.W. (1971) Cataclastic Rocks. Geol Surv Professional Paper 687, U S  
838 Government Print Office, Washington Library of Congress Catalog No. 71-  
839 611932; 1971.

840 Hooper, P.R., Hawkesworth, C.J. (1993) Chemical characteristics of island arc  
841 basalts. *J Petrol.* 1993; 34:1203–46

842 Hsü, K.J. (1974) Melanges and their distinction from olistostromes. In: Dott RH,  
843 Shaver RH (eds) Modern and ancient geosynclinal sedimentation. *Soc Econ*  
844 *Paleontol Mineral Spec Publ* 19: 321-333

845 Ichikawa, H., Yamamoto, S., Kawai, K., Kameyama, M. (2016) Estimate of  
846 subduction rate of island arcs to the deep mantle. *J Geophys Res Solid Earth.*  
847 2016; 121:5447–60.

848 Jacobshagen, V., Risch, H., Roeder, D. (1976) Die Eohellenische Phase. Definition  
849 und Interpretation. *Zeitschr Deutsche Geol Gesell.* 1976;127: 133–45.

850 Jacobshagen, V., (1986) Geologie von Griechenland. In: Beiträge Zur Regionalen  
851 Geologie der Erde Band 19. Gebrüder Bornträger, Berlin, 363 pp

852 Katrivanos, E., Kiliyas, A., Mountrakis, D. (2013) Kinematics of deformation and  
853 structural evolution of the Paikon Massif (Central Macedonia, Greece): A  
854 Pelagonian tectonic window? *N. Jb. Geol. Paläont. Abh.* 269/2, 149–171

855 Kay, R.W., Hubbard, N.J. (1978) Trace elements in ocean ridge basalts. *Earth*  
856 *Planet Sci Lett.* 38:95–116.

857 Kelepertsis, A. (1974) Geological structure of Alonnisos and Peristera islands. *Z dt*  
858 *geol Ges*;125: 225–36.

859 Kendall, G.St.C., Schlager, W. (1981) Carbonates and relative changes in sea level.  
860 In: Cita MB, Ryan WBF (eds) Carbonate platforms of the passive-type  
861 continental margins, present and past. *Mar Geol* 44: 181–212

862 Kiliyas, A., Frisch, W., Avgerinas, A., Dunkl, I., Falalakis, G., Gawlick, H-J. (2010)  
863 Alpine architecture and kinematics of deformation of the northern Pelagonian  
864 nappe pile in the Hellenides. *Austrian Journal of Earth Sciences* Volume  
865 103/1 4-28

866 Kockel, F. (1979) in: Die Vardar- (Axios-) Zone. Jacobshagen, V., Geologie von  
867 Griechenland, Gebrüder Borntraeger Berlin-Stuttgart, pp. 150-168.

868 Lallemand, S., Funicello, F., (2009) editors: Royden, Leigh H. (et al.) Subduction  
869 with Variations in Slab Buoyancy: Models and Application to the Banda and  
870 Apennine Systems. *Subduction zone geodynamics*; 35. Springer-Verlag,  
871 Berlin, Heidelberg, 272pp. ISBN 978-3-540-87974-9

872 Matarangas, D. (1992) Geological investigations of Skopelos island (North  
873 Sporades, Greece). D 188 (Diss. Freie Universität Berlin) Berichte des  
874 Forschungszentrums Jülich, 2684,157.

875 Meléndez, G., Ramajo, J., Bello, J., D'Arpa, C., Di Stefano, P., Fermeli, G.,  
876 Karakitsios, V., Mallarino, G., Mindszenty, A., Scherreiks, R., Zarcone, G.  
877 (2007) Palaeogeographic and palaeontologic event across the Tethys, in the  
878 Submediterranean and Mediterranean platforms at the Callovian-Oxfordian

879 transition. XXIII Jornadas de la Sociedad Espanola de Paleontologia  
880 (Caravaca de la Cruz, Libro de Resumenes:139–140

881 Meneghini, F., Marroni, M., Moorw, J.C., Pandolfi, L., Rowe, C.D. (2009) The  
882 processes of underthrusting and underplating in the geologic record: structural  
883 diversity between the Franciscan Complex (California), the Kodiak Complex  
884 (Alaska) and the Internal Ligurian Units (Italy). *Geol. J.* 44: 126–152

885 Mercier, J. (1968) Etude geologique des zones Internes des Hellenides en  
886 Macedoine centrale. Contribution à l'étude du metamorphisme et de l'  
887 évolution magmatique des zones internes des Hellenides. – *Annales*  
888 *Géologique des Pays Héliéniques* 20, 1-739.

889 Mercier, J., Vergely, P., Geological Map of Greece 1.50.000 - Sheet Arnissa (1988)  
890 Institute of Geology and Mineral Exploration, Athens

891 Mercier, J., Vergely, P., Geological Map of Greece 1.50.000 - Sheet Edhessa (1984)  
892 Institute of Geology and Mineral Exploration, Athens

893 Mercier, J. L., Vergely, P. (1972) Le mélanges ophiolitiques de Macédoine (Grèce) :  
894 décrochements d'âge anté-Crétacé supérieur. *Z. Deutsch, geol. Ges.*,  
895 Hannover, 123, 469-489.

896 Mercier, J.L., Vergely, P., 2002. The Paikon massif revisited, comments on the Late  
897 Cretaceous e paleogene geodynamics of the Axios-Vardar Zone. How many  
898 Jurassic ophiolitic basins? (Hellenides, Macedonia, Greece). *Bull. Geol. Soc.*  
899 *Greece* 34/6, 2099-2112. doi: org/10.12681/bgsg.16852.

900 Michail, M., Pipera, K., Koroneos, A., Kiliyas, A., Ntaflos, T. (2016) New perspectives  
901 on the origin and emplacement of the Late Jurassic Fanos granite, associated  
902 with an intra-oceanic subduction within the Neotethyan Axios-Vardar Ocean.  
903 Published online: 26 March 2016 Springer-Verlag Berlin Heidelberg 2016

904 Norton, W.H. (1917) A Classification of Breccias. *The Journal of Geology*, Vol. 25,  
905 No. 2, 160-194

906 Norton, I. O. (1999) Global plate reconstruction model report. Texas (USA):  
907 Exxon Mobil Exploration

908 Pearce, J.A., Cann, J.R. (1973) Tectonic setting of basic volcanic rocks determined  
909 using trace element analyses. *Earth Planet Sci Lett.* 1973; 19:290–300.

910 Perfit, M.R., Gust, D.A., Bence, A.E., Arculus, R.J., Taylor, S.R., (1980) Chemical  
911 characteristics of island-arc basalts: Implications for mantle sources.  
912 *Chemical Geology* Volume 30, Issue 3, 227-256

913 Photiades, A., Carras, N., Bortolotti, V., Fazzuoli, M. (2018) The late Early  
914 Cretaceous transgression on the laterites in Vourinos and Vermion massifs  
915 (western Macedonia, Greece). *Bulletin of the Geological Society of Greece*  
916 40(1):182

917 Robertson, A. (2004) Development of concepts concerning the genesis and  
918 emplacement of Tethyan ophiolites in the Eastern Mediterranean and Oman  
919 regions. *Earth Sci Rev* 66:331–387

920 Robertson, A.H.F., Trivić, B., Đerić, N., Bucur, I. (2013) Tectonic development of the  
921 Vardar ocean and its margins: Evidence from the Republic of Macedonia and  
922 Greek Macedonia. *Tectonophysics* 595–596, 25–54

- 923 Roddick, J.C., Cameron, W.A., Smith, A.G. (1979) Permo-Triassic and Jurassic  
924 40Ar/39Ar ages from Greek ophiolites and associated rocks. *Nature* 279:788–  
925 790
- 926 Saccanni, E., Photiades, A., Santato, A., Zeda, O. (2008a) New evidence for supra-  
927 subduction zone ophiolites in the Vardar zone of northern Greece:  
928 Implications for the tectonic-magmatic evolution of the Vardar ocean basin  
929 *Ofioliti*, 2008, 33 (1), 65-85
- 930 Saccanni, E., Bortolotti, V., Marroni, M., Pandolfi, L., Photiades, A., Principi, G.  
931 (2008b) The Jurassic association of backarc basin ophiolites and calc-alkaline  
932 volcanics in the Guevgueli complex (Northern Greece): Implications for the  
933 evolution of the Vardar Zone. *Ofioliti* 33 (2), 209-227
- 934 Saccanni, E., Chiari, M., Bortolotti, V., Photiades, A., Principi, G. (2015) Geochemistry  
935 of volcanic and subvolcanic rocks and biostratigraphy on radiolarian cherts  
936 from the Almopias ophiolites and Paikon unit (Western Vardar, Greece).  
937 *Ofioliti* 40,1-25. <https://doi.org/10.4454/ofioliti.v40i1.432>.
- 938 Scherreiks, R. (1998) The evolution of a passive margin in response to plate  
939 tectonics, eustasy, and an advancing ophiolite nappe (Jurassic, NE-Evvoia,  
940 Greece). *Terra Nostra* 98: 72-73
- 941 Scherreiks, R. (2000) Platform margin and oceanic sedimentation in a divergent and  
942 convergent plate setting (Jurassic, Pelagonian Zone, NE Evvoia, Greece). *Int*  
943 *J Earth Sci* 89:90–107
- 944 Scherreiks, R., Bosence, D., BouDagher-Fadel, M., Meléndez, G., Baumgartner,  
945 P.O. (2010) Evolution of the Pelagonian carbonate platform complex and the  
946 adjacent oceanic realm in response to plate tectonic forcing (Late Triassic and  
947 Jurassic), Evvoia, Greece. *Int J Earth Sci* 99:1317–1334
- 948 Scherreiks, R., Meléndez, G., Fermeli, G., Baumgartner, P.O., BouDagher-Fadel, M.,  
949 Bosence, D. (2011) A time-transgressive ophiolite-platform collision (late  
950 Middle Jurassic to Early Cretaceous, Pelagonian zone, Evvoia, Greece).  
951 *Fragile Earth: GV-GSA meeting, LMU München Paper 19-9*
- 952 Scherreiks, R., Meléndez, G., BouDagher-Fadel, M., Fermeli, G., Bosence, D. (2014)  
953 Stratigraphy and tectonics of a time-transgressive ophiolite obduction onto the  
954 eastern margin of the Pelagonian platform from Late Bathonian until  
955 Valanginian time, exemplified in northern Evvoia, Greece, *Int. J. Earth Sci.*,  
956 103, 2191-2216.
- 957 Scherreiks, R., Meléndez, G., BouDagher-Fadel, M., Fermeli, G., Bosence, D.  
958 (2016) The Callovian unconformity and the ophiolite obduction onto the  
959 Pelagonian carbonate platform of the Internal Hellenides. *Bulletin of the*  
960 *Geological Society of Greece*, vol. L; Proceedings of the 14th Intern.  
961 Congress, Thessaloniki, May 2016
- 962 Scherreiks, R., BouDagher-Fadel, M. (2020a) Tectono-stratigraphic correlations  
963 between Northern Evvoia, Skopelos and Alonnisos, and the postulated  
964 collision of the Pelagonian carbonate platform with the Paikon forearc basin  
965 (Pelagonian-Vardar zones, Internal Hellenides, Greece). *UCL Open*
- 966 Scherreiks, R., BouDagher-Fadel, M. (2020b) The closure of the Neotethys in two  
967 episodes: as a result of Late Jurassic to Early Cretaceous obduction and  
968 Early Paleocene collision, based on surface geology and tomographic models

969 (Internal Hellenides, Greece) Conference: Tectonics, geodynamics, and  
970 paleogeography of the Alpine-Himalayan orogen from the Earth's mantle to its  
971 surface at: Utrecht virtual oral presentation 26.08.2020 Session 3.3 ID 112  
972 Schmid, S.M., Bernoulli, D., Fügenschuh, B., Matenco, L., Schefer, S., Schuster, R.,  
973 et al. (2008) The Alpine-Carpathian-Dinaridic orogenic system: correlation and  
974 evolution of tectonic units. *Swiss J Geosci.* 101:139–83.  
975 Schmid, S.M., Fügenschuh, B., Kounov, A., Matenco, L., Nievergelt, P., Oberhänsli,  
976 R., et al. (2020) Tectonic units of the Alpine collision zone between Eastern  
977 Alps and western Turkey. *Gondwana Res.* 78:308–374.  
978 Sengör, A.M.C., Natal'in, B.A. (1996) Paleotectonics of Asia: fragments of a  
979 synthesis, in: *The Tectonic Evolution of Asia*, eds Yin A, Harrison T.M., 486–  
980 640, Cambridge University Press.  
981 Sharp, I.R., Robertson, A.H.F. (1994) Late Jurassic–Lower Cretaceous oceanic crust  
982 and sediments of the eastern Almopias Zone, NW Macedonia (Greece);  
983 implications for the evolution of the eastern “Internal” Hellenides. *Bull Geol  
984 Soc Greece* 30:47–61  
985 Sharp, I. R. & Robertson, A. H. F. (1998) Late Jurassic-Lower Cretaceous oceanic  
986 crust and sediments of the Eastern Almopias Zone, NW Macedonia (Greece);  
987 implications for the evolution of the Eastern 'Internal' Hellenides. *Bulletin of  
988 the Geological Society of Greece*, 30(1), 47-61.  
989 Sharp, I.R., Robertson, A.H.F. (2006) Tectonic-sedimentary evolution of the western  
990 margin of the Mesozoic Vardar Ocean: evidence from the Pelagonian and  
991 Almopias zones, northern Greece. In: *Tectonic development of the Eastern  
992 Mediterranean Region*. Robertson AHF, Mountrakis D (Eds.), *Geol. Soc.  
993 London Spec. Publ.*, 260: 373-412.  
994 Simantov, J., Economou, C., Bertrand, J. (1991) Metamorphic rocks associated with  
995 the Central Euboea ophiolite (southern Greece): some new occurrences. In:  
996 Malpus J, Moores EM, Panayiotou A, Xenophontos C (eds) *Ophiolites,  
997 oceanic crustal analogies. Proc Symp Troodos 1987*, *Geol Surv Dept  
998 Nicosia/Cyprus*, pp 285-293  
999 Schlager, W., (2000) Sedimentation rates and growth potential of tropical, cool-water  
1000 and mud-mound carbonate systems. In *Insalaco, E., Skelton, P. W., and  
1001 Palmer, T. J. (eds.), Carbonate Platform Systems: Components and  
1002 Interactions*. London: The Geological Society, pp. 217–227.  
1003 Spakman, W., van der Lee, S., van der Hilst, R.D. (1993) Travel-time tomography of  
1004 the European^Mediterranean mantle down to 1400 km, *Phys. Earth planet.  
1005 Inter.*, 79, 3-74.  
1006 Spray, J.G., Roddick, J.C (1980) Petrology and Ar geochemistry of some Hellenic  
1007 subophiolite metamorphic rocks. *Contrib Mineral Petrol*72:43–55  
1008 Spray, J.G., Bebie, J., Rex, D.C., Roddick, J.C. (1984) Age constraints on the  
1009 igneous and metamorphic evolution of the Hellenic±Dinaric ophiolites. *Geol  
1010 Soc Lond Spec Publ* 17 : 619±627  
1011 Stais, A., Ferriere, J., Caridroit, M., De Wever, P., Clement, B., Bertrand, J. (1990)  
1012 Donnees nouvelles sur l'histoire ante-obduction (Trias- Jurassique) du  
1013 domaine d'Almopias (Macedoine, Grece). *Comptes Rendus de l'Academie de  
1014 Sciences, Serie II*, 310, 1275-1480.

- 1015 Stampfli, G.M., Borel, G.D. (2004) The TRANSMED transects in space and time:  
1016 Constraints on the paleotectonic evolution of the Mediterranean domain, in  
1017 The TRANSMED Atlas: the Mediterranean Region from Crust to Mantle. eds  
1018 Cavazza, W., Roure, F., Spakman, W., Stampfli, G.M., Ziegler, P.A., Springer  
1019 Tranos, M. D., Plougarlis, A. P., Mountrakis, D. M. (2007) A new consideration  
1020 about the Almopias-Paikon boundary based on the geological mapping in the  
1021 area of Nerostoma-Lakka (Central Macedonia, Greece)  
1022 Proceedings of the 11th International Congress, Athens, May,  
1023 Ustaszewski, K., Kounov, A., Schmid, S.M., Schaltegger, U., Krenn, E., Frank, W.,  
1024 Fügenschuh, B. (2010) Evolution of the Adria-Europe plate boundary in the  
1025 northern Dinarides: from continent–continent collision to back-arc extension.  
1026 *Tectonics* 29:1-34  
1027 van der Meer, D.G., van Hinsbergen, D.J.J., Spakman, W. (2018) Atlas of the  
1028 underworld: Slab remnants in the mantle, their sinking history, and a new  
1029 outlook on lower mantle viscosity. *Tectonophysics* 723, 309–448  
1030 van Hinsbergen, D.J.J., Hafkenscheid, E., Spakman, W., Meulenkamp, J.E., Wortel,  
1031 M.J.R. (2005) Nappe stacking resulting from subduction of oceanic and  
1032 continental lithosphere below Greece. *Geology* 33, 325–328.  
1033 van Hinsbergen, D.J.J., Torsvik, T.H., Schmid, S.M., Matenco, L.C., Maffione, M.,  
1034 Gürer, D., Vissers, R.L.M. (2019) Companion paper. Orogenic architecture of  
1035 the Mediterranean region and kinematic reconstruction of its tectonic evolution  
1036 since the Triassic. *Gondwana Res.*  
1037 Vermeesch, P. (2006) Tectonic discrimination diagrams revisited. *Geochem*  
1038 *Geophys Geosyst Am Geophys Union* 7(6):1–55  
1039 Woodcock, N.H., Mort, K. (2008). Classification of fault breccias and related fault  
1040 rocks. *Geological Magazine*, 145(3), 435-440.  
1041 Zimmerman, J., Ross, J.V. (1976) Structural evolution of the Vardar root zone,  
1042 northern Greece. *Bull Geol Soc Am* 87: 1547-1550  
1043

## 1044 **Figure Captions**

1045

1046 **Fig. 1: Neotethys lithosphere** The oceanic lithosphere of the Dinarides through the Hellenides and  
1047 Taurides, and beyond, represents remnants of the northern branch of the Neotethys (following  
1048 Stampfli and Borel 2004, and numerous researchers in Schmid et al. 2020). Our study areas are in  
1049 Evvoia and the Northern Sporades, and in the “Vardar zone” of Greek Macedonia. Fieldwork was  
1050 carried out in the Vardar zone and Northern Evvoia in September and October 2020 and Evvoia and  
1051 the Northern Sporades in previous years  
1052

1053

1054 **Fig. 2 Palaeogeography and evolution of the Vardar ocean** (a) altered after Stampfli and Borel,  
1055 2004; (b) altered after Schmid et. al. 2008; Gallhofer et al 2017 and Van Hinsbergen et al. 2019, in  
1056 Schmid et al, 2020)

1057 a) The Vardar domain of the Northern Tethys ocean evolved out of the Maliac and Paleotethys in  
1058 Permo-Triassic time.

1059 b) The Vardar ocean was situated between continental Adria (including Korab-Pelagonia) and Serbo-  
1060 Macedonian Europe. The paleogeography infers that early Middle Jurassic intra-oceanic subduction  
1061 led the obduction of the Eohellenic ophiolite onto eastern Pelagonia. Subsequently, Vardar ocean  
1062 lithosphere subducted beneath the Paikon island arc and led to the crash of eastern Pelagonia with  
1063 the island arc. See text.

1064

1064 **Fig. 3** Seismic tomographic images below the Central Hellenides

- 1065 a) Map sketch of the Hellenides shows the position of the NE-SW vertical section through the mantle  
1066 below the Central Hellenides c).  
1067 b) Seismic tomographic images (BSE models, ascertained from Hafkenscheid 2004) of horizontal  
1068 sections through the mantle at 6 different depths, showing iso-density contours.  
1069 c) The vertical section through the BSE models. The sketch schematically depicts perturbation  
1070 “clouds” containing the lithospheric “slabs” (see e)). Slab X has sunk about 900km, slab Y has sunk  
1071 about 400km.  
1072 d) Vertical sections depicting the mantle eastwards of the Hellenides show that there are two sinking  
1073 lithospheric slabs.  
1074 e) The perturbations appear to bulge with depth in the mantle, suggesting that subducted slabs  
1075 undergo vertical compression and folding? in which case, only the minimum widths of the original  
1076 slabs can be estimated.

1077  
1078 **Fig. 4 Overview tectonic sections of the study areas** (nomenclature “Almopias, Paikon and  
1079 Peonian” units after Kockel, 1979).

1080 a) western part of section shows obducted ophiolite, composed of serpentinite, peridotite, basalt,  
1081 gabbro and radiolarian chert, which was obducted together with tectonic mélangé over the Pelagonian  
1082 carbonate platform (Scherreiks 2000). The Elias formation has been interpreted as a relict of a supra-  
1083 subduction island arc complex (Scherreiks et al. 2014). Bauxite was deposited during the Callovian  
1084 (Scherreiks et al. 2016) (Table 1a 5 and 6). The eastern part of section a) shows overthrust,  
1085 supposed Vardar, Cretaceous platform carbonates and mylonitized ocean floor mélangé (devoid of  
1086 serpentinite). This nappe overlies eroded Upper Triassic dolomite (Scherreiks and BouDagher-Fadel  
1087 2020). Section b), shows the Vardar zone between the Guevgueli ophiolite complex and Pelagonian  
1088 ophiolite near Arnissa. Exposures of Pelagonia-derived ophiolite s. str. occur in the western and  
1089 central parts of the Almopias zone near Karydia and Lyki/Klisochori; Serpentinite is not found in the  
1090 eastern Almopias zone, the Krania-Nea zoi units, or the units of the Paikon sub-zone (see also Fig.  
1091 6).

1092  
1093 **Fig. 5 Overview geologic map of Skopelos and Alonnisos in the Northern Sporades** (based on  
1094 Matarangas 1992; Kelepertsis 1974 and Scherreiks and BouDagher-Fadel 2020), The Cretaceous  
1095 limestone formation of Alonnisos and Skopelos lies tectonically emplaced, together with a sheared  
1096 mélangé of metamorphic ocean-floor basalt and radiolarian chert, on top of an erosional disconformity  
1097 over Pelagonian Upper Jurassic limestone on Alonnisos and Upper Triassic dolomite on Skopelos. It  
1098 has been postulated that the tectonic emplacement took place during Paleocene time as Pelagonia  
1099 underthrust the Cretaceous forearc basin of the Vardar volcanic arc (Scherreiks and BouDagher-  
1100 Fadel 2020).

1101  
1102 **Fig. 6 Geologic overview map of the Vardar and adjacent Pelagonian zone** (based on Mercier  
1103 and Vergely 1988 and 1984; Katrivanos et al. 2013; Georgiadis et al. 2016; and own field work). The  
1104 Pelagonian zone is in an underthrust position relative to the Cretaceous carbonate platform of the  
1105 Vardar zone (Georgiadis et al. 2016) (B-B'). Imbricated ophiolite and Jurassic limestone are exposed  
1106 in a window extending from Margarita to Veria. Metamorphosed Pelagonian limestone is exposed in  
1107 the Gandach antiform of the Paikon sub-zone near Livadia. The tectonic section A-A' is shown in  
1108 Figure 4b. The formations between the Gandach marble and the Theodoraki limestone is a composite  
1109 mélangé

1110  
1111 **Fig. 7 Chondrite-normalized REE and ternary discrimination diagrams**

- 1112 a. LREE enriched samples, probably IABs.  
1113 b. Flat REE and LREE depleted samples, most likely MORBs (see text).  
1114 c. Discrimination diagrams: Vardar-zone data (AFMs are also shown for Evvoia and the Northern  
1115 Sporades). The AFM from Perfit and others (1980) shows the plots of 1170 IABs (also the dashed  
1116 red line area in the Vardar diagram, encompassing only a few of the Vardar meta-basalts).

1117  
1118 **Fig. 8 Composite tectono-stratigraphic synopsis:**

- 1119 a) Evvoia and the Northern Sporades were overthrust by the Eohellenic ophiolite which was  
1120 subsequently deeply eroded and transgressed by ~Cenomanian orthoconglomerates. On the

1121 Northern Sporades, the ophiolite and Lower Cretaceous had been removed by erosion before being  
1122 underthrust beneath the Vardar-zone sheet during Paleocene time. b) Likewise, the Vardar zone was  
1123 underthrust by Pelagonia, which carried remnants of Eohellenic ophiolite and possibly Cenomanian  
1124 orthoconglomerates. c) schematic section through the Vardar ocean between Pelagonia and Serbo-  
1125 Macedonia indicating the widths (km) of oceanic lithosphere (see seismic tomography).  
1126 Legend: 1) Cretaceous and Paleocene carbonates. 2) mélange including Triassic radiolarite and  
1127 basalt, pyroclastic rocks, and carbonate slices. 3) Upper Jurassic (Pelagonian slices) and lower  
1128 Cretaceous Theodoraki carbonate slices. 4) Pelagonian ophiolite s. str. 5) Pelagonian Jurassic  
1129 carbonates 6) Pelagonian upper Triassic dolomite 7) Crystalline basement of Pelagonia. D1-D3  
1130 deformations (see text)

1131

### 1132 **Fig. 9 Palaeogeography and time-laps cartoons**

1133 a) The Vardar ocean was situated between two passive margins, continental Adria (including Korab-  
1134 Pelagonia) and Serbo-Macedonian Europe. Early Middle Jurassic intra-oceanic subduction led to the  
1135 demise of about 1200 km of Vardar lithosphere and to the obduction of about 200 km of the  
1136 Eohellenic ophiolite onto eastern Pelagonia. Subsequently, about 1700km of Vardar ocean  
1137 lithosphere subducted beneath the Paikon (east Vardar) island arc, followed by the crash of eastern  
1138 Pelagonia with the island arc, and finally (c) to the collision of Pelagonia with Serbo-Macedonia.  
1139 b) This time-laps cartoon shows the demise of the Vardar ocean in 7 stages. The Vardar ocean slabs  
1140 are shown as they reach their present position shown in Fig. 3c. It is important to note that the Earth's  
1141 curvature has been neglected in the graphic. This creates distortion in the lower mantle making it  
1142 appear wider than it should be.

#### 1143 *Time schedule of subduction*

- 1144 1) The Vardar ocean existed during Late Triassic time verified by radiolarians associated with pillow  
1145 basalt (Table 1a Carnian-Norian).
- 1146 2) Intra-oceanic subduction was in progress around Toarcian to Aalenian time (180–170 Ma), based  
1147 on the metamorphic age of subduction-zone amphibolite mélange (Roddick et al. 1979; Spray and  
1148 Roddick 1980). Plate polarity, however, had already changed from divergence to convergence, during  
1149 the Late Triassic, testified by the subsidence of the Rhaetian-Sinemurian peritidal carbonate platform  
1150 and change to the subtidal platform of Pliensbachian and Toarcian time (Scherreiks et al. 2010)  
1151 (Table 2a Rhaetian-Pliensbachian). Subduction of slab (x) continued through the Middle Jurassic,  
1152 verified by late Middle Jurassic radiolarians in ophiolite mélange in Evvoia (Danelian and Robertson  
1153 2001; Scherreiks et al. 2014).
- 1154 3) Platform uplift, erosion and bauxite deposition occurred during the Callovian (Meléndez et al. 2007;  
1155 Scherreiks et al. 2016), presumably due to the crash of the Eohellenic arc with the Pelagonian  
1156 platform (Callovian unconformity *ibid.*), causing upwarping of the carbonate platform. This stress  
1157 communicated across the east Vardar ocean causing subduction between east Vardar and Serbo-  
1158 Macedonia.
- 1159 4) As the Eohellenic ophiolite advanced, the carbonate platform subsided below the CCD during  
1160 Kimmeridgian-Berriasian time while back arc spreading was taking place in Guevgueli.
- 1161 5) The final Eohellenic ophiolite emplacement takes place about Valanginian time. The west Vardar  
1162 slab x breaks off and sinks, the Pelagonian platform rises and deep erosion of the Eohellenic nappe  
1163 takes place. The Cretaceous carbonate platform evolves on top of volcanic debris of the forearc basin  
1164 and accretionary wedge. The east Vardar slab (y) continues to subduct.
- 1165 6) Pelagonia crashes with the arc, underthrusts the Cretaceous carbonate platform and volcanic arc,  
1166 and the Guevgueli back arc basin.
- 1167 7) Pelagonia crashes with Serbo-Macedonia while the Vardar slab breaks off and subsides.

1168

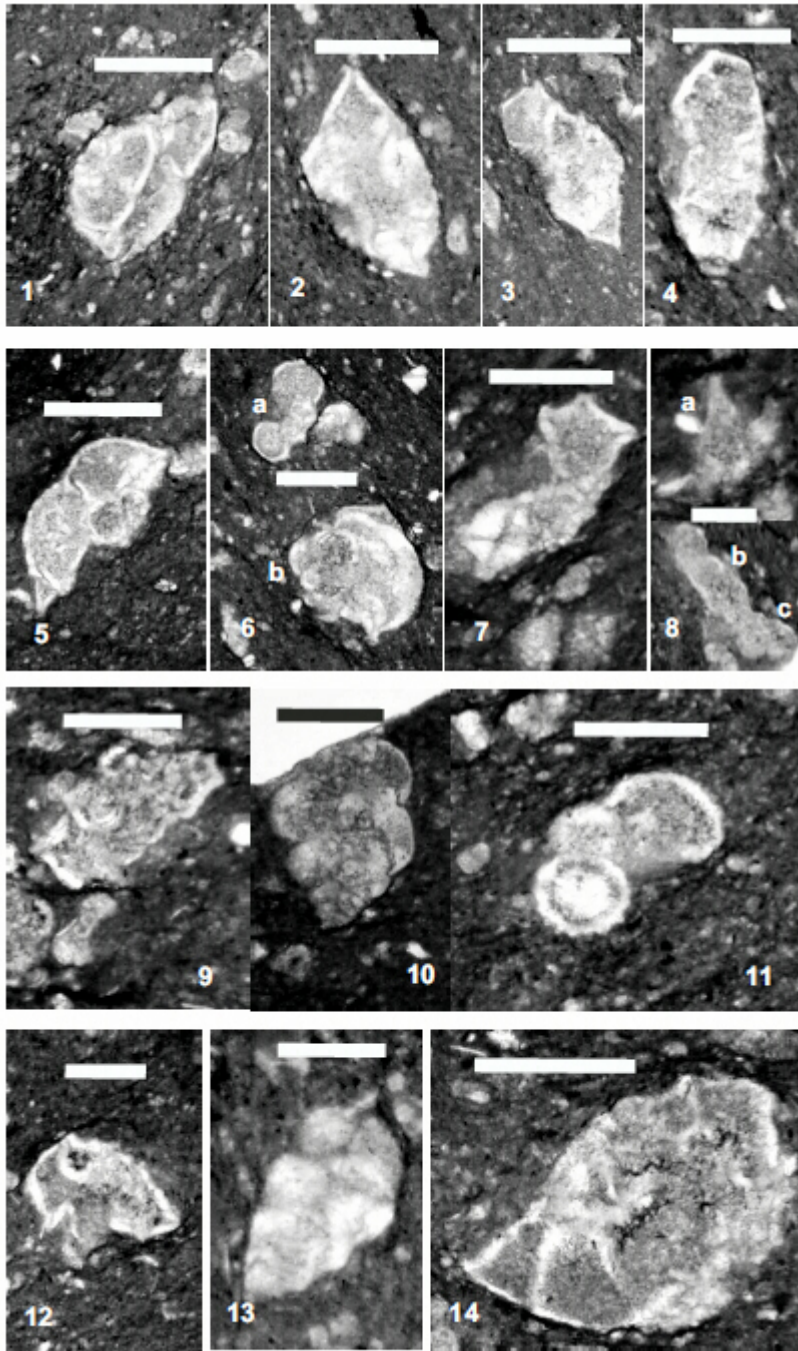
1169 c) The cartoon shows the final episode of Vardar ocean subduction. Pelagonia crashes and  
1170 underthrusts the arc and the Vardar slab breaks off. Pelagonia crashes with Serbo-Macedonia which  
1171 initiates folding and renewed thrust faulting.

1172

1173

1174

1175



1177

1178 Plate 1

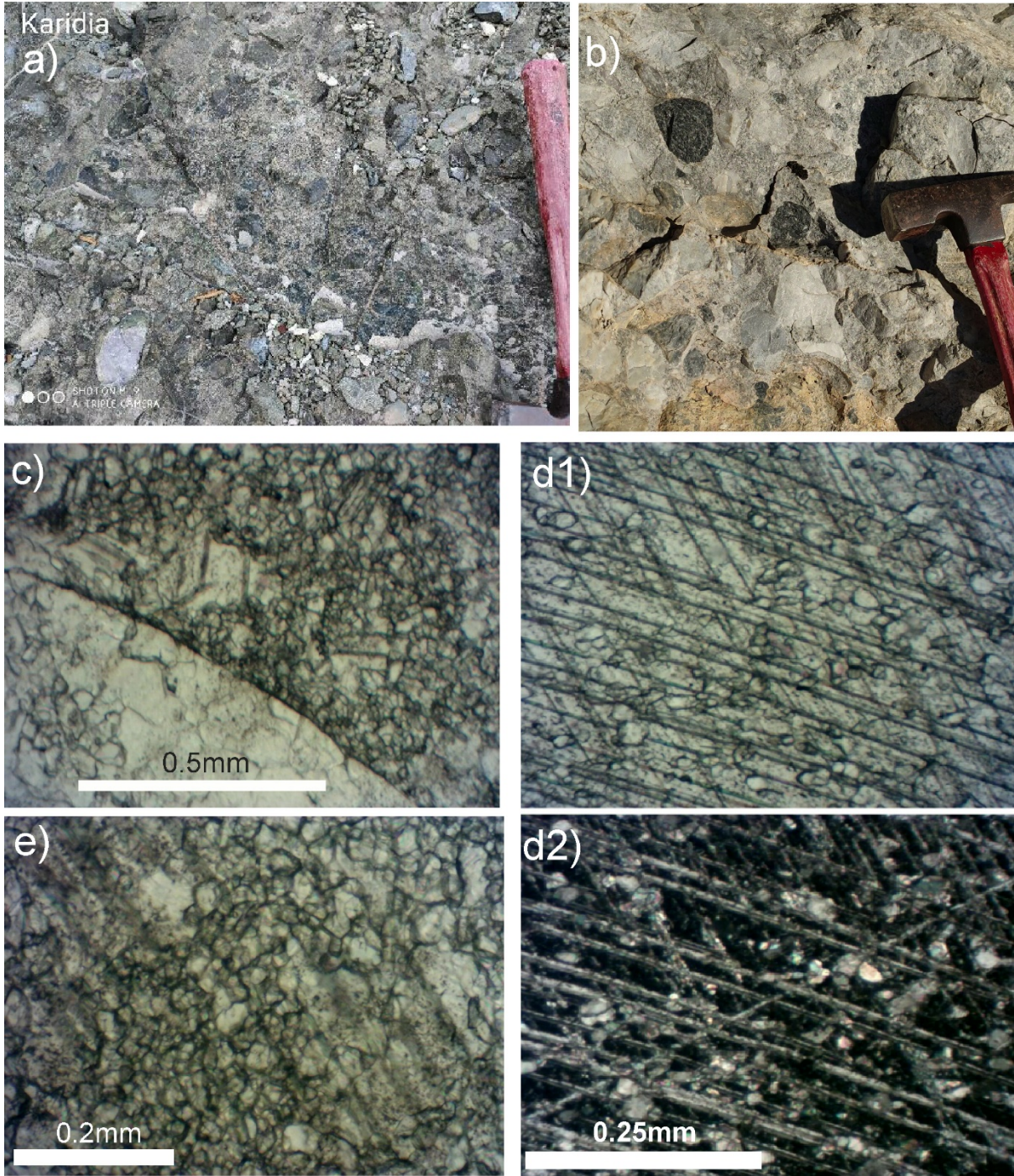
1179

1180 ?Scale bars: Figs 1 – 14

1181

1182 Fig. 1. *Contusotruncana fornicata* (Plummer).1183 Fig. 2. *Globotruncanita stuarti* (De Lapparent).1184 Fig. 3. *Globotruncana arca* (Cushman).1185 Fig. 4. *Globotruncana linneiana* (d'Orbigny).1186 Fig. 5. *Radotruncana subspinososa* (Pessagno)-1187 Fig. 6. a) *Rugoglobigerina hexacamerata* Brönnimann, b) *Radotruncana subspinososa* (Pessagno),1188 Fig. 7. *Globotruncana aegyptiaca* Nakkady.

- 1189 Fig. 8. a) *Schackoia* sp., b) *Ventilabrella glabrata* (Cushman), c) *Rugoglobigerina hexacamerata*  
 1190 Brönnimann.  
 1191 Fig. 9. *Globotruncana lapparenti* Bolli.  
 1192 Fig. 10. *Heterohelix dentata* (Stenestad).  
 1193 Fig. 11. *Rugoglobigerina rugosa* (Plummer).  
 1194 Fig. 12. *Globotruncana rosetta* (Carsey).  
 1195 Fig. 13. *Heterohelix carinata* (Cushman).  
 1196 Fig. 14. *Globotruncanita atlantica* (Caron).  
 1197



- 1198  
 1199  
 1200  
 1201  
 1202

1203  
1204 Plate 2a  
1205 a. Field photo: breccio-conglomeratic ophiolite mélange in west Almopias, near Karydi  
1206 b. Field photo: breccio-conglomeratic carbonate mélange in west Almopias near Nisi  
1207 c. Photomicrograph: rounded grain of limestone and adjacent matrix of micro-breccia without cement.  
1208 d1 and d2 Photomicrographs: neomorphic calcite (parallel and crossed nicols) in the matrix of 2b,  
1209 showing palimpsest relic matrix grains and twinning planes.  
1210 e-Photomicrograph: matrix of 2b showing initial palimpsest texture of growing neomorphic calcite in  
1211 the matrix with recognisable twin planes  
1212  
1213  
1214  
1215  
1216  
1217  
1218  
1219  
1220  
1221  
1222  
1223  
1224  
1225  
1226  
1227  
1228  
1229  
1230  
1231  
1232  
1233  
1234  
1235  
1236  
1237  
1238  
1239  
1240  
1241  
1242  
1243  
1244  
1245  
1246  
1247  
1248  
1249  
1250

<p><b>Table 1a biostratigraphy of Evvoia and Northern Sporades</b> (BouDagher-Fadel 2008; Scherreiks 2000; Scherreiks et al. 2010, 2014; Scherreiks and BouDagher-Fadel 2020a)</p>
<p><b>Pelagonian carbonate platform</b></p> <p><b>1. Rhaetian-Hettangian: peritidal/subtidal</b> ? <i>Aulotortus</i> sp., “<i>Aulotortus friedli</i>”, <i>Auloconus permodisoides</i>, <i>Grillina</i> sp. “<i>Vidalina</i>” <i>martana</i></p> <p><b>2. Sinemurian-Early Pliensbachian: shallow warm reef environment</b> <i>Siphovalvulina colomi</i>, <i>Siphovalvulina gibraltarensis</i>, <i>Duotaxis metula</i>, <i>Lituosepta recoarensis</i>, <i>Riyadhella praeregularis</i>. <i>Lituosepta compressa</i>, <i>Riyadhella praeregularis</i>, <i>Palaeodasyclus mediterraneus</i>, <i>Pseudocyclammina liasica</i>, <i>Lituosepta recoarensis</i></p> <p><b>3. Aalenian-Bathonian: shallow water environment</b> <i>Mesoendothyra croatica</i> Gusic’</p> <p><b>4. Middle to Upper Jurassic: shallow water environment</b> BouDagher-Fadel 2008 <i>Neokilianina rahonensis</i></p>
<p><b>5. Bathonian-Callovian foraminifera suite: shallow warm reef environment This limestone occurs below the below the bauxite</b> <i>Pseudomarssonella bipartita</i>, <i>Redmondoides medius</i>, <i>Andersenolina elongata</i>, <i>Riyadhella</i> sp. <i>Ammobaculites</i> sp., <i>Trocholina</i> sp., <i>Palaeodasyclus cf. mediterraneus</i>, <i>Pseudopfenderina</i> sp., <i>Everticyclammina</i> sp., <i>Siphovalvulina</i> sp., <i>Riyadhoides</i> sp.</p> <p><b>6. Callovian-Oxfordian foraminifera suite on top of laterite: shallow reef environment</b> <i>Chablaisia</i> sp., <i>Septatrocholina banneri</i>, <i>Andersenolina elongata</i>, <i>Andersenolina</i> sp., <i>Palaeodasyclus</i> sp</p>
<p><b>7. Upper Jurassic shallow patch-reef environment</b> <i>Protopeneroplis striata</i>, <i>Parurgonina caeinensis</i>, <i>Thaumatoporella parvovesiculifera</i>, <i>Actinostromaria tokadiensis</i></p> <p><b>8. Late Berriasian-Early Valanginian: shallow reef environment</b> <i>Cladocoropsis mirabilis</i>, <i>Zergabriella embergeri</i></p>
<p><b>9. Late Cretaceous transgression in Evvoia, Maastrichtian: outer neritic environment</b> <i>Plummerita</i> aff. <i>hantkeninoides</i>, <i>Idalina</i> aff. <i>antiqua</i>, <i>Hippurites</i> sp., <i>Planorbulina cretae</i>: on a rudist clast (Campanian).</p>
<p><b>Cretaceous carbonate platform of the Northern Sporades</b></p> <p><b>10.1 Albian to Santonian: shallow reef environment</b> <i>Nezzazatinella picardi</i>, <i>Nezzazata convexa</i>, <i>Dicyclina schlumbergeri</i></p> <p><b>10.2 Late Santonian to Maastrichtian: reef/forereef environment</b> <i>Rotorbinella</i> sp., <i>Orbitoides</i> sp., <i>Lithocodium</i> sp., <i>Lithocodium aggregatum</i>, rudists</p> <p><b>10.3 Early Paleocene: shallow reef environment</b> <i>Kathina</i> sp., <i>Daviesina</i> sp., <i>Lockhartia</i> sp</p>
<p><b>Radiolarians in Evvoia</b></p> <p><b>11. Ophiolite sheet:</b> Scherreiks et al. 2014, determined in co-operation with P. O. Baumgartner, Gingins and Schauner (Baumgartner et al. 1995).</p> <p><b>11.1 Carnian to Lower Norian:</b> <i>Annulotriassocampe</i> ? sp., <i>Castrum</i> ? sp., <i>Corum</i> ? sp., <i>Capnuchosphaera</i> cf. <i>crassa</i> <i>Capnuchosphaera</i> sp.</p> <p><b>11.2 Elias complex, Middle to Late Jurassic:</b> <i>Spongocapsula hooveri</i>, <i>Parvicingula dhimenaensis</i> s.l. <i>Transhuum brevicostatum</i>, <i>Protunuma</i> sp., <i>Sethocapsa</i> sp.</p>
<p><b>12. Ophiolite mélange</b> (Danelian and Robertson 2001; Gingins and Schauner 2005) <b>Middle Bathonian to Lower Callovian</b> <i>Parvicingula dhimenaensis</i> ssp., <i>Mirifusus fragilis</i> s.l., <i>Transhuum maxwelli</i> gr., <i>Tricolocapsa plicarum</i> s.l.</p>

1251  
1252  
1253  
1254  
1255  
1256  
1257  
1258  
1259  
1260

**Table 1a** Biostratigraphic data, Evvoia and the Northern Sporades

1261  
1262  
1263  
1264

<p><b>Table 1b West and Central Almopias</b> After Mercier and Vergely 1988 Updated and additional age and palaeoenvironmental determinations (BouDagher-Fadel et al., 2015, 2018a, 2018b)</p>
<p><b>1. West Almopias</b>  <b>1.1 Late Maastrichtian (Maastr, 2): inner neritic environment</b> Planktonic foraminifera <i>Abathomphalus mayaroensis</i>, <i>Globotruncana Stuarti</i>, <i>Contusotruncana contusa</i>, <i>Globotruncana arca</i> and <i>Globotruncana linneiana</i> and the larger benthic foraminifera <i>Orbitoides medius</i>  <b>1.2 Santonian-early Campanian: shallow reef/intertidal environments.</b> The Hippuritidae, <i>Vaccinites atheniensis</i></p>
<p><b>2 Kato Grammatiko Pyrgi: Cenomanian (Cen. 1): forereef/inner neritic environment.</b> Planktonic foraminifera <i>Rotalipora appenninica</i> and larger benthic foraminifera <i>Nezzazata simplex</i></p>
<p><b>3. Kerassia Campanian-Maastrichtian (Camp. 3b-Maast 2), : inner to outer neritic environment</b>  <i>Globotruncana arca</i> [= <i>G. convexa</i>], <i>Globotruncanita</i> gr. <i>stuarti-stuartiformis</i></p>
<p><b>4 Kerassia – Nisi – Kedronas</b>  <b>4.1 Campanian (3, 77.0-72.1Ma): Inner to outer neritic planktonic foraminifera in micritic wackestone:</b> <i>Radotruncana subspinoso</i>; <i>Heterohelix dentata</i>, <i>H. spp.</i>; <i>Globotruncana lapparenti</i>, <i>G. aegyptiaca</i>, <i>G. ventricosa</i>, <i>G. linneiana</i>, <i>G. rosetta</i>, <i>G. arca</i>; <i>Contusotruncana fornicata</i>; <i>Ventilabrella glabrata</i>; <i>Rugoglobigerina rugosa</i>, <i>R. hexacamerata</i>; <i>Globotruncanita atlantica</i>, <i>Gl. stuarti</i>, <i>Gl. sp.</i>; <i>Schackoia</i> sp.; <i>Globotruncanella</i> sp.; <i>Archaeoglobigerina blowi</i>.  <b>4.2 Aptian (Apt. 1-4a): reefal to inner neritic environment depositional depths of between 10 and 50m.</b> The presence of the larger benthic foraminifera <i>Palorbitolina discoidea</i> Gras (Barremian to Aptian), <i>Palorbitolina lenticularis</i>, indicate Aptian 1-4a age 125-115 Ma (see BouDagher-Fadel and Price, 2019).</p>
<p><b>5. Kerassia – Kedronas - Kato Grammatiko Campanian-Maastrichtian (Camp.3-Maast): reefal (rudist debris) to reworked in outer neritic</b> <i>Globotruncana arca</i>, <i>Globotruncanita stuarti</i>, <i>Globotruncana linneiana</i> [= <i>G. tricarinata</i>]  <b>5.1 Late Santonian (Sant.2): outer neritic</b> <i>Globotruncana lapparenti</i>, <i>Globotruncana arca</i> [= <i>G. convexa</i>], <i>Marginotruncana coronata</i>, <i>Sigalia deflaensis</i>  <b>5.2 Early Santonian (Sant. 1): outer neritic</b> <i>Praeglobotruncana turbinata</i>, <i>Sigalitroncana sigali</i>, <i>Marginotruncana coronata</i>, <i>Globotruncana linneiana</i> <i>Globotruncana lapparenti</i>.</p>
<p><b>6 Jurassic exposures in the Kerassia-Nisi area (Pelagonian origin) Oxfordian-Early Cretaceous: low energy environment</b> <i>Stylosmilia</i> cf. <i>miehelini</i>, <i>Thecosmilia</i> cf. <i>langi</i>, <i>Cladocoropsis mirabilis</i>, <i>Dermosmilia</i> sp. and <i>Schizosmilia</i> cf. <i>rollieri</i> indicate a? Late Oxfordian-? Early Kimmeridgian age (in Sharp and Robertson 2006)</p>
<p><b>7. Central Almopias (Maragarita and Klissochori limestones on top of Jurassic mélange) with “conglomeratic” lenses</b>  <b>7.1 Flamouria, (east of Edessa) Early Santonian: outer neritic</b> <i>Marginotruncana coronata</i>, <i>Globotruncana arca</i> [= <i>G. convexa</i>, <i>Marginotruncana marginata</i>. The shallow water Early Cretaceous. larger benthic foraminifera, <i>Orbitolina</i> sp. are reworked into the pelagic assemblages.  <b>7.2 Messimeri (beneath Central Almopias mélange south of Edessa)</b> <i>Cladocoropsis</i> sp. Indicates Late Jurassic age and Pelagonian</p>

1265  
1266  
1267  
1268  
1269  
1270  
1271

**Table 1b** Biostratigraphic data, west and central Almopias

1272  
1273  
1274  
1275

<b>Table 1c East Almopias and Paikon</b> (after Mercier and Vergely 1984) updated age and environment (BouDagher-Fadel et al.,2015)
<b>1. Nea Zoi</b> <b>1.1 Cenomanian (Cen. 3): outer neritic environment.</b> <i>Rotalipora cushmani</i> and <i>Praeglobotruncana stephani</i> <b>1.2 Late Santonian-early Campanian (Sant.2-Camp.2): inner to outer neritic</b> <i>Globotruncanita elevata</i> , <i>Globotruncana convexa</i> , <i>Globotruncana arca</i> , <i>Orbitoides media</i>
<b>?2. Krania-Mavrolakkos Unit.</b> Radiolarian determinations (? P. De Wever & H. YiLing; in Sharp & Robertson 1998; 2006) ages ranging from Callovian to Early Cretaceous?
<b>3. Krania Unit: Mid-Oxfordian to Valanginian</b> Radiolarians reported by Stais (1994).
<b>4. Vryssi Unit and Nea Zoi Unit:</b> basalts are overlain by radiolarite of <b>Late Triassic</b> (Stais et al. 1990).
<b>Paikon</b> <b>5- Theodoraki unit</b> <b>5.1 Late Maastrichtian(Maast. 2-3): outer neritic</b> <i>Globotruncana linneiana</i> , <i>Contusotruncana contusa</i> , <i>Globotruncana arca</i> <b>5.2 Maastrichtian (Maast. 2-3): outer neritic</b> <i>Globotruncana arca</i> [= <i>G. convexa</i> ], <i>Globotruncana linneiana</i> [= <i>G. tricarinata</i> ] <i>Globotruncana calciformis</i> , <i>Contusotruncana contusa</i> indicate late Maastrichtian age. <b>5.3 Early Campanian (Camp 1-2): outer neritic</b> <i>Globotruncanita stuartiformis</i> indicates Campanian Santonian <i>Marginotruncana marginata</i> indicates an early Santonian age reworked into early Campanian assemblage. <b>5.4 Earl Cenomanian (Cen. 1): reef/inner neritic</b> <i>Orbitolina</i> gr. <i>Concava</i> , <i>Nezzazata</i> sp., <i>Cuneolina</i> sp., <i>Cycloloculina</i> sp., <i>Pseudolituonella</i> sp. (see BouDagher-Fadel, 2018a)
<b>6. Griva-Khromni mélange</b> (from numerous researchers in Katrivanous et al. 2013). <b>6.1 Aptian-Early Albian</b> <i>Mesorbitolina</i> sp., <i>Sabaudia minuta</i> <b>6.2 Late Jurassic to Early Cretaceous</b> <i>Actinoporella</i> sp., <i>Pseudocyclamina</i> sp., <i>Cuneolina</i> sp., <i>Cladocoropsis mirabilis</i> , nerineid gastropods

1276  
1277  
1278  
1279  
1280  
1281  
1282  
1283  
1284  
1285  
1286

**Table 1c** Biostratigraphic data, east Almopias and Paikon

1287

1288

Analyte Symbol	SiO2	Al2O3	Fe2O3(T)	MnO	MgO	CaO	Na2O	K2O	TiO2	P2O5	LOI	Total	Sc	Be	V	Ba	Sr	Y	Zr	Cr	Co	Ni	Cu	
Unit Symbol	%	%	%	%	%	%	%	%	%	%	%	%	ppm	ppm	ppm	ppm	ppm							
Lower Limit	0.01	0.01	0.01	0.001	0.01	0.01	0.01	0.01	0.001	0.01			0.01	1	1	5	2	2	1	2	20	1	20	10
Method Code	FUS-ICP	FUS-ICP	FUS-ICP	FUS-ICP	FUS-ICP	FUS-ICP	FUS-ICP	FUS-ICP	FUS-ICP	FUS-ICP	GRAV	FUS-ICP	FUS-MS	FUS-MS	FUS-MS	FUS-MS								
14	79.94	4.34	10.05	0.106	0.63	0.36	0.26	0.47	0.387	0.38	3.23	100.2	6	< 1	66	100	135	17	173	90	7	50	20	
16	74.42	9.37	2.99	0.049	0.97	3.56	1.77	1.72	0.368	0.08	4.49	99.78	7	1	49	243	152	15	101	160	6	40	10	
25	52.87	16.74	11.07	0.166	2.92	7.63	4.97	0.03	0.649	0.02	2.57	99.64	42	< 1	301	8	85	16	26	< 20	33	20	380	
26	38.64	4.34	3.05	0.117	2.75	26.13	0.67	0.47	0.370	0.08	22.73	99.34	8	< 1	56	92	463	12	53	400	10	140	10	
36	62.02	13.26	6.96	0.175	7.60	0.82	0.01	2.47	0.641	0.13	6.45	100.5	15	2	120	245	9	17	121	250	28	170	20	
38	50.18	12.85	11.24	0.157	4.53	6.57	2.47	0.03	2.085	0.24	10.41	100.8	41	< 1	336	36	78	35	129	100	29	40	110	
41	54.06	14.10	11.45	0.190	2.85	5.59	4.52	0.46	1.494	0.17	5.97	100.8	35	< 1	303	87	187	29	82	80	38	60	20	
44	43.12	13.66	12.54	0.148	6.93	9.31	2.68	0.02	2.235	0.25	9.96	100.9	43	< 1	375	12	117	36	133	90	40	50	20	

Analyte Symbol	Zn	Ga	Ge	As	Rb	Nb	Mo	Ag	In	Sn	Sb	Cs	La	Ce	Pr	Nd	Sm	Eu	Gd	Tb	Dy	Ho	Er
Unit Symbol	ppm	ppm	ppm	ppm	ppm	ppm	ppm	ppm	ppm	ppm	ppm	ppm	ppm	ppm	ppm	ppm							
Lower Limit	30	1	1	5	2	1	2	0.5	0.2	1	0.5	0.5	0.1	0.1	0.05	0.1	0.1	0.05	0.1	0.1	0.1	0.1	0.1
14	80	7	1	195	10	6	3	0.6	< 0.2	1	9.5	< 0.5	19.3	29.1	4.14	16.3	3.5	1.65	2.9	0.5	2.8	0.6	1.5
16	30	10	< 1	< 5	62	4	< 2	< 0.5	< 0.2	1	1.4	2.0	15.7	30.6	3.76	14.7	3.1	0.69	2.5	0.4	2.6	0.6	1.6
25	70	15	2	< 5	< 2	< 1	< 2	< 0.5	< 0.2	< 1	0.7	< 0.5	1.5	3.6	0.55	2.9	1.2	0.42	1.8	0.4	2.8	0.7	2.1
26	50	4	< 1	6	15	2	< 2	< 0.5	< 0.2	1	0.5	1.4	6.8	13.9	1.72	6.8	1.6	0.49	1.8	0.3	1.9	0.4	1.1
36	80	15	2	< 5	92	10	< 2	< 0.5	< 0.2	2	< 0.5	3.0	19.3	35.5	4.79	18.5	4.3	1.06	3.8	0.6	4.0	0.8	2.2
38	500	15	< 1	10	< 2	3	< 2	< 0.5	< 0.2	1	0.5	< 0.5	4.1	11.9	2.00	11.5	4.1	0.97	5.8	1.1	7.2	1.5	4.4
41	50	15	1	8	4	< 1	< 2	< 0.5	< 0.2	< 1	1.1	1.6	4.2	12.0	2.00	10.5	3.8	1.29	4.9	0.9	5.6	1.2	3.6
44	100	17	1	< 5	< 2	3	< 2	< 0.5	< 0.2	1	0.7	< 0.5	5.7	15.5	2.66	14.1	4.5	1.83	6.4	1.2	7.6	1.6	4.4

Analyte Symbol	Tm	Yb	Lu	Hf	Ta	W	Tl	Pb	Bi	Th	U
14	0.25	1.6	0.32	3.5	0.4	1	0.3	78	< 0.4	4.7	2.0
16	0.24	1.5	0.26	2.4	0.4	< 1	0.3	11	< 0.4	5.4	1.3
25	0.35	2.4	0.42	0.9	< 0.1	< 1	< 0.1	< 5	< 0.4	0.6	0.3
26	0.16	1.1	0.17	1.1	0.2	< 1	< 0.1	< 5	< 0.4	1.4	0.5
36	0.31	2.1	0.32	2.9	0.7	1	0.4	< 5	< 0.4	8.2	1.6
38	0.66	4.3	0.67	3.3	0.2	1	< 0.1	263	< 0.4	0.3	0.5
41	0.53	3.5	0.55	2.3	< 0.1	2	< 0.1	< 5	< 0.4	0.4	0.4
44	0.64	4.1	0.60	3.2	0.2	< 1	< 0.1	< 5	< 0.4	0.3	0.9

Activation Laboratories Ltd. Report

FUS-ICP, FUS-MS: inductively coupled plasma mass spectrometry

1289

1290 **Table 2a** Geochemistry of major and trace elements for the Vardar zone  
 1291 (Fusion-Inductively Coupled Plasma Mass Spectrometry and Fusion  
 1292 Mass Spectrometry)  
 1293

	SiO2	Al2O3	Fe2O3(T)	MnO	MgO	CaO	Na2O	K2O	TiO2	P2O5	LOI	Total	Sc	Be	V	Cr	Co	Ni	Cu	Zn	Ga	Ge	As
1 Ev metabas	53.08	13.19	7.30	0.226	10.44	2.80	2.56	1.37	1.147	0.15	6.46	98.74	37	< 1	212	240	35	110	120	110	11	1	< 5
2 Ev serp Nikol	36.86	0.59	8.24	0.089	40.71	0.20	0.01	< 0.01	0.009	< 0.01	11.94	98.66	8	< 1	31	2440	112	2500	< 10	160	< 1	< 1	< 5
3 Ev perid Mour	42.13	1.08	8.91	0.130	45.25	1.32	0.03	0.01	0.010	< 0.01	-0.20	98.67	12	< 1	47	3040	112	2440	50	120	1	< 1	< 5
4 A1 basalt Agnati	55.42	16.16	9.92	0.111	5.43	1.03	6.11	0.03	0.611	0.04	4.83	99.71	46	< 1	338	< 20	34	20	160	90	15	< 1	18
5 A8 basalt Geor	61.36	16.66	7.44	0.077	4.11	0.32	1.25	2.95	0.815	0.11	4.43	99.55	18	2	137	210	17	110	30	110	21	2	8
6 S5 Bas Paloiki	47.33	15.64	12.26	0.160	7.43	5.78	3.64	0.28	1.959	0.22	5.11	99.81	41	< 1	361	240	42	110	50	120	16	1	< 5
Elias 01	70.94	13.60	5.32	0.121	1.63	0.11	0.42	3.83	0.599	0.06	3.85	100.5	14	2	124	320	16	19	116	70	20	50	70
Elias 02	72.35	11.81	4.72	0.087	1.54	0.14	0.31	3.62	0.499	0.05	3.29	98.4	12	2	106	271	14	12	94	60	18	70	70
Elias 03	53.48	16.03	11.26	0.112	2.55	6.23	6.53	0.13	1.174	0.26	2.61	100.4	38	< 1	333	43	94	18	73	830	31	220	30

	Rb	Sr	Y	Zr	Nb	Mo	Ag	In	Sn	Sb	Cs	Ba	La	Ce	Pr	Nd	Sm	Eu	Gd	Tb	Dy	Ho	Er
1 Ev metabas	31	76	20	80	8	< 2	< 0.5	< 0.2	< 1	< 0.5	1.4	86	10.4	27.4	2.97	12.6	3.3	0.94	3.9	0.7	4.0	0.8	2.4
2 Ev serp Nikol	< 2	2	< 1	< 2	< 1	< 2	< 0.5	< 0.2	< 1	< 0.5	< 0.5	3	< 0.1	< 0.1	< 0.05	< 0.1	< 0.1	< 0.05	< 0.1	< 0.1	< 0.1	< 0.1	< 0.1
3 Ev perid Mour	< 2	< 2	< 1	< 2	< 1	< 2	< 0.5	< 0.2	< 1	< 0.5	< 0.5	3	< 0.1	< 0.1	< 0.05	< 0.1	< 0.1	< 0.05	< 0.1	< 0.1	< 0.1	< 0.1	< 0.1
4 A1 basalt Agnati	< 2	103	17	28	< 1	< 2	< 0.5	< 0.2	< 1	< 0.5	0.6	22	1.9	5.2	0.66	3.2	1.3	0.30	2.0	0.4	2.6	0.6	1.9
5 A8 basalt Geor	130	58	23	162	12	< 2	0.5	< 0.2	3	< 0.5	3.6	462	23.0	49.1	5.54	20.8	4.5	0.97	4.1	0.7	4.3	0.8	2.4
6 S5 Bas Paloiki	7	32	38	153	4	< 2	< 0.5	< 0.2	1	0.5	< 0.5	23	5.4	15.6	2.72	14.3	4.6	1.44	6.7	1.1	7.2	1.5	4.3
Elias 01	70	19	< 1	< 5	137	9	< 2	< 0.5	< 0.2	2	< 0.5	5.5	36.3	78.0	8.04	30.2	5.3	1.04	4.1	0.6	3.9	0.8	2.4
Elias 02	70	14	< 1	< 5	109	8	< 2	< 0.5	< 0.2	2	1.4	4.2	28.1	55.4	6.28	23.3	3.6	0.60	2.1	0.4	2.2	0.5	1.5
Elias 03	100	9	1	6	2	15	< 2	< 0.5	< 0.2	< 1	1.7	< 0.5	9.7	19.1	2.57	11.0	2.6	0.90	2.7	0.5	2.7	0.6	1.7

	Tm	Yb	Lu	Hf	Ta	W	Tl	Pb	Bi	Th	U
1 Ev metabas	0.35	2.2	0.32	1.5	0.8	2	< 0.1	< 5	< 0.4	2.5	0.5
2 Ev serp Nikol	< 0.05	< 0.1	< 0.01	< 0.2	< 0.1	< 1	< 0.1	< 5	< 0.4	< 0.1	< 0.1
3 Ev perid Mour	< 0.05	< 0.1	< 0.01	< 0.2	< 0.1	< 1	< 0.1	7	< 0.4	< 0.1	< 0.1
4 A1 basalt Agnati	0.29	2.0	0.32	0.8	< 0.1	1	< 0.1	< 5	< 0.4	0.7	0.1
5 A8 basalt Geor	0.37	2.3	0.34	4.2	1.0	2	0.4	15	< 0.4	12.2	1.5
6 S5 Bas Paloiki	0.66	4.1	0.61	3.3	0.2	2	< 0.1	< 5	< 0.4	0.3	< 0.1